White Paper

SOMATOM Force

Get two steps ahead with Dual Source CT

Thomas Flohr, Bernhard Schmidt,
Juergen Merz, Peter Aulbach
Computed Tomography,
Siemens Healthcare GmbH, Forchheim, Germany

SIEMENS Healthineers

SOMATOM Force

Get two steps ahead with Dual Source CT

SOMATOM Force is a two-tube (Dual Source) CT that has been completely redesigned, to the very last detail. Built with over 40 years of experience developing CT imaging systems and over eleven years of Dual Source CT expertise, this high-end system truly shows what is possible today with CT innovations and clinical outcomes. Together with the successful SOMATOM Drive, it forms the Dual Source platform from Siemens Healthineers. This white paper offers more in-depth insights into the technology behind the system and explains what will be possible in clinical research and routine.

New gantry, new tube, new detector, new iterative reconstruction

SOMATOM Force is a third-generation Dual Source CT (DSCT) system that was completely redesigned with several innovations that will excite the scientific CT imaging community for the coming years. Overall, SOMATOM Force is the combination of a new gantry design which contains two new high-end X-ray sources (Vectron™ tube), a new detector design (Stellar^{Infinity} detector), and the next level of iterative reconstruction – ADMIRE (Advanced Modeled Iterative Reconstruction).

The new gantry design facilitates faster rotation times (0.25 s), in combination with a high speed pitch of up to 3.2. With regards to scan speed, where SOMATOM Definition Flash had already set the industry benchmark with remarkable 458 mm/s volume acquisition, SOMATOM Force now exceeds this with unmatched 737 mm/s.

Another major improvement included in the new CT system is the Vectron™ tube. The focal spot of this tube remains small, precise and stable, even at a high tube current (mA). Therefore the spatial resolution of up to 24 lp/cm can be achieved in different scan modes. Furthermore, this tube has the capabilities to deliver a high tube current of up to 1,300 mA even at low kV from 70–90 kV. At the upper end, the tube can now facilitate up to 150 kV. Furthermore, kV settings can be changed in steps of 10 kV. Finally, a new moveable Tin Filter has been incorporated into the tube housing which can be used in selected scan modes to further reduce the dose. The power for all this comes together with a new generator power of 2 x 120 kW.

In 2012, the Stellar detector marked the first step towards a fully integrated detector, reducing electronic noise and heat dissipation while improving image quality and enabling lower dose levels. Now with the Stellar^{Infinity} detector, SOMATOM Force pushes the boundaries of detector technology once again. The integration of the detector module has reached new levels: For the first time, signal processing can be performed right underneath the photodiode. Compared to previous CT generations, the amount of detector rows has also increased from 64 rows to 96 rows per detector in combination with more channels (920) per row. By using a diagonal flying focal spot, the system acquires 384 slices (2 x 192) even at the highest gantry rotation times. On top, the detector has a combination of a 2D focused anti-scatter grid, which collimates and focuses in two directions simultaneously, plus a spherical detector design. This is called a 3D anti-scatter grid.

To address the emerging challenges in CT image reconstruction, Siemens Healthineers has now released new state-of-the art iterative reconstruction technology called ADMIRE: Advanced Modeled Iterative Reconstruction. The basic principles will be described in this white paper and can be understood as comprising of three steps. ADMIRE uses advanced statistical weighting of all projections in the raw-data space. Next, an advanced regularization intelligently separates noise from actual anatomical structures. Finally, ADMIRE generates a complete modeling of the CT geometry, scanner components, and characteristics. With five different strength levels to choose from, ADMIRE reduces noise, improves spatial resolution, and reduces artifacts at lower dose levels.

First clinical results

The combination of the new gantry design, the two Vectron™ tubes with a stronger generator power, two Stellar^{Infinity} detectors, and ADMIRE, form a new high-end CT imaging system that has already generated an impact of over 200 peer-reviewed publications (see selected overview in the addendum) Nevertheless, it still leaves room for further research in the future. Furthermore, the system already has over 300 installations (end of October 2017), which demonstrates its capacities in university hospitals, emergency care units, regional hospitals, cardiac centers, pediatric hospitals, and outpatient centers all over the world.

Increased spatial resolution enables enhanced detail visualization in CT angiography, and in bone and inner ear imaging. For example, Beeres et al. (2016) see an improved visual delineation of the intimal flap in Standford type A and B dissections, especially in the far ends of the dissection membrane. Gassenmeier et al. (2014) concluded that SOMATOM Force may be a valid alternative for detecting in-stent restenosis. Meyer et al. (2015) have already shown that bone imaging can be performed with significantly improved spatial resolution, and that diagnostic information for the middle/inner ear can be gained with 50% less dose.

The fast scan speed at high temporal resolution (66 ms) is beneficial for cardiac CT, CT angiography (CTA), pediatric CT, and for treating patients who are un-cooperative or struggle to hold their breath. Gordic et al. (2014) have shown that the Turbo Flash Spiral mode delivers robust coronary CT angiographies in one heart beat with heart rates up to 70 bpm. For patients with high and unstable heart rates and arterial fibrillation, the sequential mode offers an easy way to get diagnostic images even with the most challenging patients. Wielander et al. (2016) came to the conclusion that high-pitch dual source CTA might eliminate the need for ECG-triggering of the ascending aorta, while still providing excellent image quality. For pediatrics, the ultra-high pitch can be used to scan without sedation and in combination with 70 kV at a significantly reduced radiation dose (Hagelstein et al. 2015). With its fast volume coverage, the system can also scan elderly patients and unconscious patients who are often unable to follow breathing instructions properly.

With the release of SOMATOM Force, Siemens Healthineers has set a new path in CT imaging by bringing low kV imaging into clinical routine – not only for children and slim adults, but also for regular and slightly obese adults. This is especially beneficial for patients with renal insufficiency, since it leaves room to decrease either the radiation dose or the amount of contrast media given, or both. For the first time, it may enable CT imaging for patients who would not usually have access to CT imaging due to their poor creatinine values. Meyer et al. (2014) have shown that coronary studies can be performed in clinical routine with 70 kV at a dose level of 0.44 mSv and with only 45 mL of contrast media. TAVI/TAVR planning can be performed with only 38 mL of contrast media (Bittner et al., 2016). Even obese patients with a BMI >40 kg/m2 can be scanned with a reduced amount of only 80 mL (Mangold et al., 2015). Finally, Meinel et al. (2014) see the potential for reducing dose levels in obese patients by up to 68%.

Another highlight is the system's new spectral pre-filtration in combination with ADMIRE, which reduces the dose in non-enhanced CT scans. This new feature can be used in low-dose lung imaging, for example, where it enables CT imaging at the dose level of conventional X-ray (Martini et al., 2016). For Gordic et al. (2014), the average dose value for the detection of pulmonary nodules can be performed with an effective radiation dose of 0.06 mSv, which produces high image quality, sensitivity, and diagnostic confidence. This innovative technique can additionally be used for low-dose CT of the paranasal sinuses with an effective dose below 0.05 mSv (Wuest et al.). Lell et al. (2015) conclude in their study that the effective dose is comparable with that of conventional radiography, and that the high image quality at even lower radiation exposure favors multidetector row CT over conebeam CT. It will be interesting to see what will develop in this field of research in the future.

Studies from second generation Dual Source CT with SOMATOM Definition Flash have already shown that Dual Source offers the best spectral separation without anan increase in radiation dose (Schenzle et al., 2010). SOMATOM Force now offers the chance to introduce new protocols with different kV pairings with 150 kV with Tin Filter (150 kV Sn) as the upper voltage for even better separation (Krauss et al., 2015). Frellesen et al. (2015) have shown that this approach can significantly improve image quality and pancreas-to-lesion contrast in the diagnosis of pancreatic adenocarcinoma while Hardie et al. (2015) suggest that the use of virtual monoenergetic reconstruction with the Mono+ algorithm at 55 keV is most suitable and should be considered for clinical routine. With a wide range of applications, Dual Energy can also be used for the identification of urinary stones when differentiating between oxalate and apatite stones. Duan et al. (2015) and Dewes et al. (2016) have already investigated and shown better outcomes with the usage of 150 kV Sn in comparison with second generation Dual Source CT. The first results with Dual Energy-based display of bone marrow in osteoporotic vertebral compression fractures also demonstrate high accordance with MR imaging (Kaup et al., 2016). The improved spectral separation presents another field of imaging with numerous opportunities for further research.

Until now, one disadvantage of dynamic CT perfusion has been the high radiation dose. SOMATOM Force enables routine use of low-kV imaging (70 kV, 80 kV) for perfusion scans up to 22 cm and dynamic imaging of up to 80 cm. The effective dose of a liver perfusion CT can be as low as a conventional 3-phase liver protocol. Haubenreisser et al. (2015) outline the potential of dynamic imaging as a new approach for evaluating peripheral arterial occlusive disease and as a highly promising technique for post-interventional EVAR follow-up examinations. They see the potential to reduce dose levels by up to 52% by shifting from 100 kV to 70 kV in dynamic imaging. They also envisage further fields of research such as preoperative dynamic CTA for patients with flap reconstruction or for a more accurate evaluation of dialysis shunts. In the area of cardiac perfusion, SOMATOM Force allows clinicians to confidently and reliably determine the hemodynamic relevance of intermediary stenosis. Thanks to the high temporal resolution of 66 ms, it is possible to perform perfusion examinations without heart rate control – both at rest and at stress with a radiation dose of ca. 3–5 mSv.

Conclusion

SOMATOM Force is the unparalleled performance class in Dual Source Computed Tomography. Together with SOMATOM Drive, it forms the new Dual Source CT platform from Siemens Healthineers. This high-end CT can be used as an individualized diagnostic tool, and is particularly beneficial in sensitive patient groups such as very young patients, patients with impaired kidney function, chronic diseases, as well as obese patients. The advantages of SOMATOM Force – unparalleled spatial resolution at low radiation dose and low contrast agent dose, fast acquisition speed to ensure minimal motion artifacts, whole organ low dose functional imaging, and extremely precise Dual Energy quantification – make it suitable for a wide range of applications.

Contents

1. Technical characteristics

SOMATOM Force is a Dual Source CT (DSCT) system that was introduced at RSNA 2013. The system is equipped with two newly developed Vectron X-ray tubes and Stellar^{Infinity} detectors at an angle of 95°, see Fig. 1. Image reconstruction is based on the new ADMIRE iterative reconstruction process. SOMATOM Force offers a unique high-pitch spiral scan mode, Turbo Flash spiral, with a scan speed of up to 737 mm/s and 66 ms temporal resolution at 0.25 s gantry rotation time. The key components of the system are described in the following sub-sections.

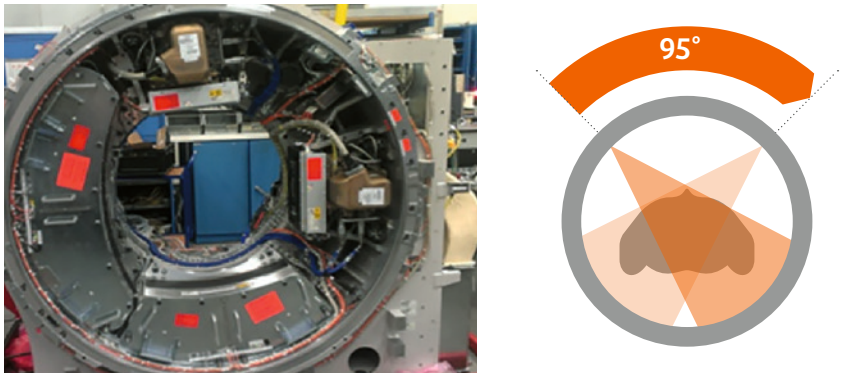

Figure 1: DSCT SOMATOM Force with two Vectron X-ray tubes and two corresponding Stellar^{Infinity} detectors at an angle of 95°.

1.1 Vectron X-ray tube

The Vectron X-ray tube (see Fig. 2) and the corresponding high-power generator offer unique performance parameters. The two Vectron X-ray tubes in SOMATOM Force provide power reserves of up to 2 x 120 kW to allow fast scanning at a high temporal resolution, with 0.25 s gantry rotation time (see section 3). The tube potential can be set between 70 kV and 150 kV in intervals of 10 kV; to date, this feature which adjusts kV to the individual patient and examination is unique in diagnostic CT. High tube power is maintained at low kV: The maximum tube current of 1,300 mA at 70 kV and 80 kV enables the dose-efficient low-kV scanning of adult and obese patients (see section 4). Figure 3 shows the available power reserves of the Vectron tube as a function of the X-ray tube voltage, compared with publicly available data for other vendors' X-ray tubes[1].

[1] *Impact Group, UK, 03/2009 at http://www.impactscan.org/reports/CEP08028.htm, and GE Discovery CT750 HD technical reference manual, 2012 at http://apps.gehealthcare.com/servlet/ClientServlet?REQ=RNEW&MODALITY=CT*

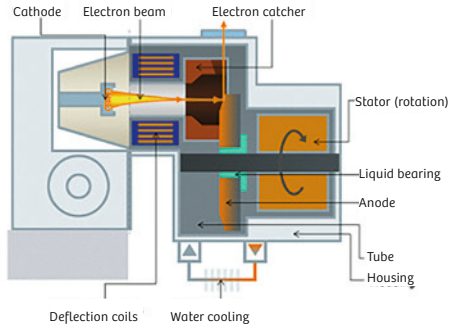

Figure 2: Diagram of the Vectron X-ray tube.
The electron catcher is a large, actively-cooled copper dome to efficiently absorb extra focal radiation which would otherwise cause focal spot blooming and degrade spatial resolution and contrast resolution.

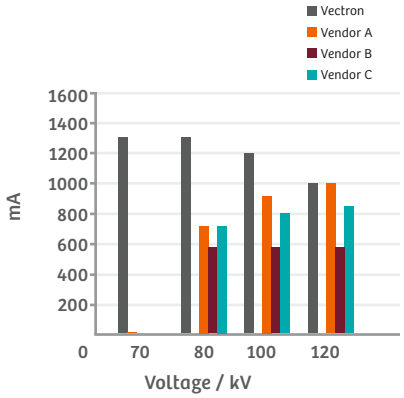

Figure 3: Tube current reserves (in mA) as a function of the X-ray tube voltage for the Vectron X-ray tube (grey bars) compared with other vendors' tubes.
Note the significantly increased power reserves of the Vectron tube at 70–100 kV, which enable dose-efficient low-kV scanning of adults and obese patients.

Thanks to the efficient electron catcher, the focal spot of the Vectron tube is very small (0.4 x 0.5 mm²) and it keeps its size regardless of the X-ray tube voltage and tube current. This avoids the usual spreading of the focal spot at a high X-ray tube power, which negatively impacts the spatial resolution and image contrasts. This has been evaluated by researchers at the Clinical Innovation Center, Mayo Clinic Rochester, Minnesota, USA (see Fig. 4).

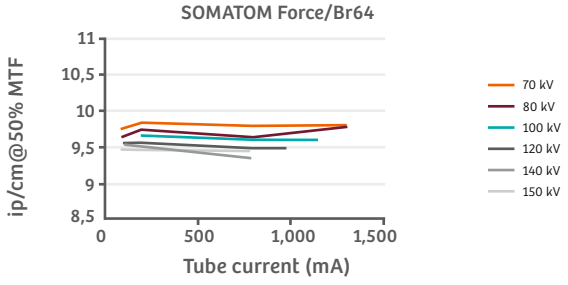

Figure 4: Spatial resolution (50% value of the modulation transfer function MTF of the regular body kernel Br64) as a function of the tube current mA at different X-ray tube voltages. Spatial resolution is practically independent of the kV setting and independent of the X-ray tube current (mA). As a result, spatial resolution is maintained even at very high tube power. Courtesy of the Clinical Innovation Center, Mayo Clinic Rochester, Minnesota, USA.

Both X-ray tubes can be operated at different tube voltage settings, enabling the acquisition of Dual Energy CT data for material discrimination and functional CT imaging. In contrast to other approaches, that offer a limited choice of scan parameters for Dual Energy CT, such as fixed tube voltages of 80 kV and 140 kV in rapid kV switching techniques, SOMATOM Force provides a wide range of Dual Energy scan modes (70 kV / 150 Sn kV, 80 kV / 150 Sn kV, 90 kV / 150 Sn kV and 100 kV / 150 Sn kV). "Sn" refers to the use of additional tin prefiltration of the high-kV X-ray spectrum to absorb lower-energy X-ray photons and to improve spectral separation

(Primak et al., 2009). The maximum tube voltage of 150 kV instead of the standard 140 kV is a further step towards improving Dual Energy performance.

SOMATOM Force also has single energy CT scan modes with tin pre-filtration, such as 100 Sn kV or 150 Sn kV. These enable non-enhanced CT scans – CT lung examinations, virtual colonoscopy, CT scans for the detection of kidney stones, or CT scans of the sinuses, for example – at very low radiation dose levels (see section 5).

1.2 Stellar^{Infinity} detector

The Stellar^{Infinity} detector comprises 96 detector rows with a collimated slice width of 0.6 mm and 920 detector channels per row. By means of a diagonal flying focal spot, which is active even at the fastest gantry rotation time of 0.25 s, the detector acquires 1,840 in-plane samples, and 192 through-plane samples in the z-direction. The in-plane spatial resolution is 30% higher than in any previous CT scanner technology. In combination with ADMIRE, and supported by the small focal spot size of the Vectron X-ray tube, image slices with a minimum slice width of 0.4 mm can be reconstructed (McCollough et al., 2013). In routine scan modes, an in-plane spatial resolution of 14–15 lp/cm is achievable even at the fastest gantry rotation time of 0.25 s (Fig. 5, left). When using a special ultra-high resolution comb (see Fig. 9a and 9b), a clinically-viable maximum in-plane spatial resolution of 26 lp/cm can be achieved (see Fig. 5, right). The cutoff frequency of the modulation transfer function (MTF) is 32 lp/cm. Note that this is the resolution level of a flat panel detector used in conventional catheter angiography. Inner ear imaging, bone imaging, as well as high-resolution lung imaging may benefit from this significantly increased spatial resolution.

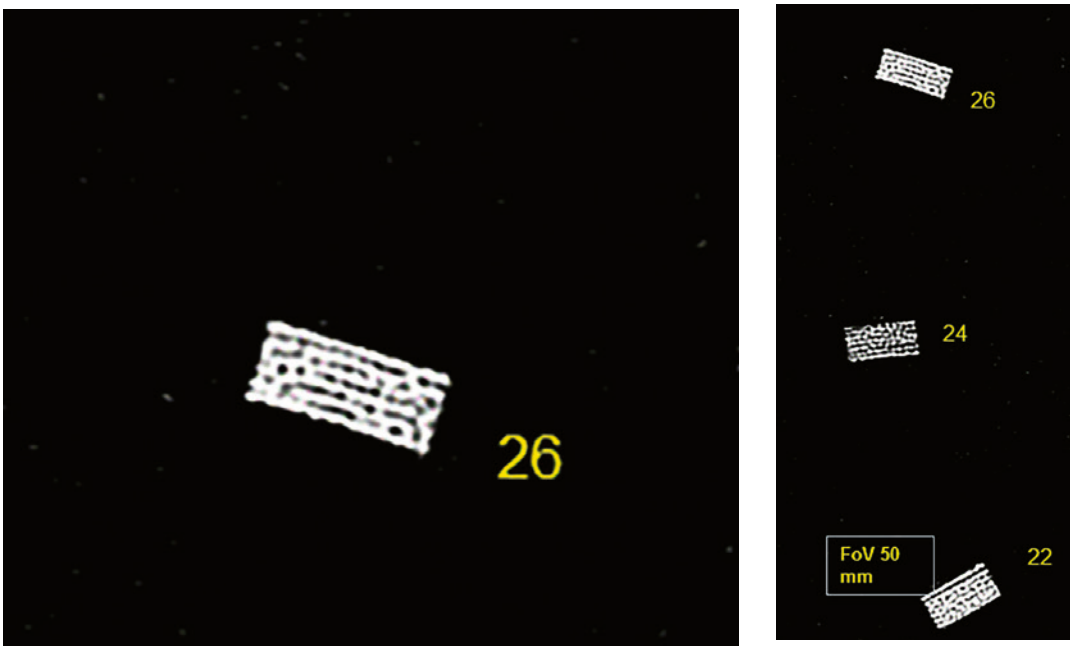

Figure 5: Demonstration of in-plane resolution using SOMATOM Force with a resolution phantom. Left: Standard scan mode. Up to 14–15 lp/cm are visible. Right: Ultra-high resolution scan mode. Up to 26 lp/cm are visible.

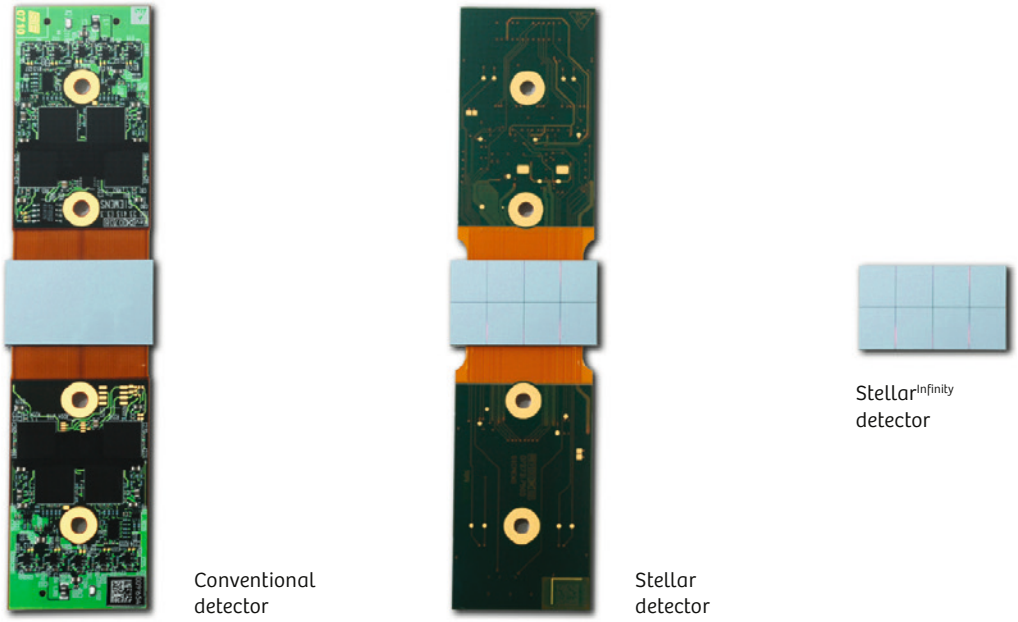

Figure 6: The evolution of the Stellar^Infinity detector. While the left-hand side shows conventional detector technology of the first generation Dual Source (SOMATOM Definition), the second generation Dual Source (SOMATOM Definition Flash) had the first integrated detector, which was called the Stellar detector (introduced in 2012). Along with SOMATOM Force, detector technology has taken the next step toward a fully integrated detector with all the signal processing sitting right underneath the photodiode.

The Stellar^Infinity detector is based on Stellar technology. It has significantly reduced detector cross-talk and low electronics noise compared with standard CT detector designs. This facilitates CT scanning at a very low radiation dose, significant radiation dose reduction in perfusion CT, and CT scanning of obese patients (Morsbach et al., 2013 and Duan et al., 2013). Using Stellar technology, Duan et al. observed "up to 40% noise reduction for a 30 cm phantom scanned using 80 kV. This noise reduction translated into up to 50% in dose reduction to achieve equivalent image noise."

Figure 7: The Stellar^Infinity technology (front and backside of the photodiode) shows the highest level in integration for reduced detector cross-talk and low electronic noise. The outcome is a significantly lower radiation dose.

Both Stellar^Infinity detectors in SOMATOM Force are equipped with two-directional anti-scatter grids, collimating both in the detector channel direction (in-plane direction) and in the detector row direction (z-axis direction, see Fig. 9a and 9b). Most medical CT scanners use one-directional collimation in the detector channel direction only. Scattered radiation causes image artifacts such as cupping and banding, and it reduces image contrasts. To restore the contrast-to-noise ratio (CNR), a higher radiation dose is needed when there is scattered radiation. Scattered radiation increases in the z-axis direction as the detector width increases.

Different types of anti-scatter collimators:

Scatter is a significant source of image artifacts in wide-cone CT. Scatter management includes both scatter rejection and scatter correction.

The common scatter rejection approach is to use an anti-scatter collimator (ASC).

- **1D anti-scatter collimator**
  The commonly known anti-scatter collimator is comprised of thin plates formed of a suitable X-ray absorbing material like lead or tungsten. These plates are focused at the X-ray focal spot and generally located between columns of detectors (z-direction) but not between rows of detectors. This collimator is referred to as a "1D" anti-scatter collimator.

Conventional CT scanners (with detector coverage not exceeding 40 mm along the patient axis) typically employ one-dimensional (1D) ASCs. These grids are quite effective for small cone angles.

- **2D anti-scatter collimator**
  In multi-slice scanners it is advantageous to have shielding between both columns and rows of detectors; both directions focus to the X-ray source. This type is called a "2D" anti-scatter collimator.

- **2D focused anti-scatter collimator plus spherical detector: The 3D collimator grid (Fig. 8)**
  A spherical detector has a sensitive area which is formed as a part of a sphere instead of a part of a cylinder, which is more common in traditional CT's. In the SOMATOM Force a spherical detector shape is combined with a 2D anti-scatter grid in the Stellar^{Infinity} detector. This innovation is called a 3D collimator grid. Technologically this is the most complex but most efficient way of preventing the negative aspects of scatter radiation.

Using a spherically shaped detector generally improves the quality of the images reconstructed from it. The 3D anti-scatter grids of SOMATOM Force efficiently reduce scattered radiation by a factor of 2–3 compared with standard anti-scatter collimation (see Fig. 10), leading to an improved CNR at a lower radiation dose.

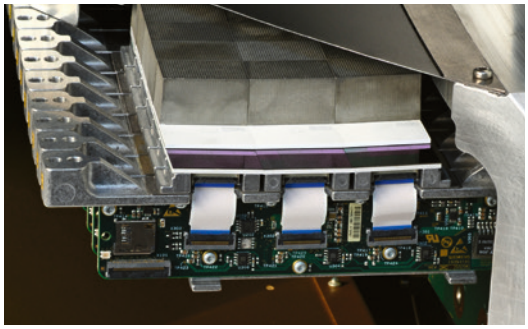

Figure 8: The spherically shaped Stellar^{Infinity} detector equipped with focused 2D anti-scatter grids. 2D anti-scatter grids characterize the new anti-scatter 3D collimator grid.

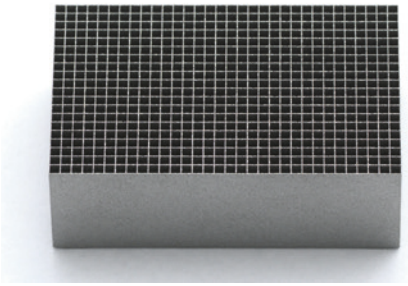

Figure 9A: One of the innovations of SOMATOM Force is the new anti-scatter 3D collimator grid.

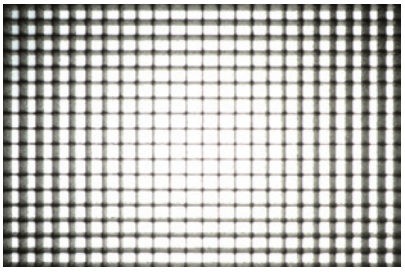

Figure 9B: Top view of the shaped anti-scatter 3D collimator grid of the spherically shaped Stellar^{Infinity} detector.

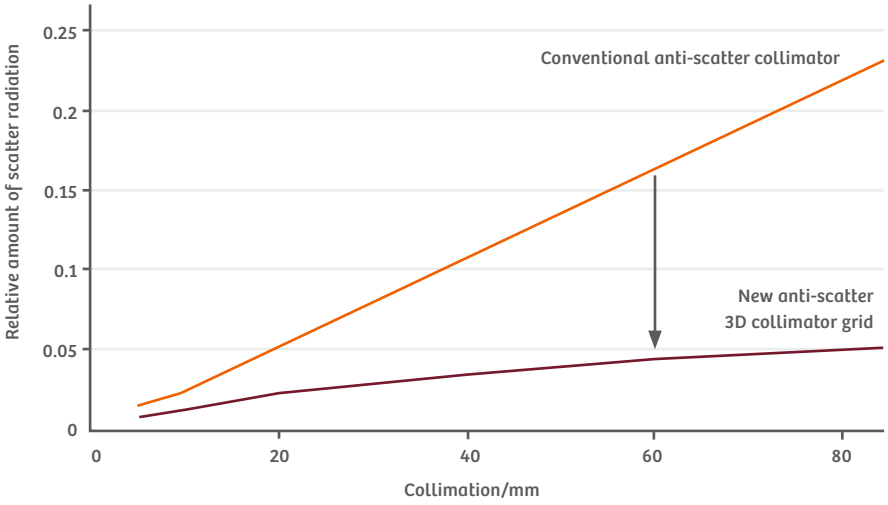

Figure 10: Reduction of scattered radiation with the new anti-scatter 3D collimator grid compared with a standard anti-scatter collimator. The z-axis collimation of SOMATOM Force is 57.6 mm.

1.3 ADMIRE: Advanced Modeled Iterative Reconstruction

Evolution of Siemens Healthineers' CT Image Reconstruction Technologies
Image reconstruction is an essential technology that every computed tomography (CT) scanner requires for operation. The function of CT image reconstruction is to translate all the acquired X-ray data (raw data) into a meaningful three-dimensional representation of the patient. The best method of image reconstruction is the so-called filtered back projection (FBP), in which measured X-ray projections are directly translated into images. Siemens Healthineers' CT scanners offer an improved three dimensional FBP, called weighted filtered back projection (WFBP), that is used daily in the clinical practice of CT worldwide. Yet WFBP does not consider statistical properties of measured X-ray projections. This means that all CT projections collected in the detectors are weighted the same, regardless of their statistical properties. For example, unreliable (e.g., noisy) projections are considered in the same manner as high-quality projections. With the increased focus on dose reduction, the aforementioned shortcoming of conventional WFBP becomes an important obstacle in further reducing the radiation dose. To address this obstacle, WFBP reconstruction has begun to be replaced by a more advanced technology known as iterative reconstruction (IR). Unsurprisingly, among the key advantages of IR is that the statistical properties of measured CT projection data can be readily incorporated into the CT image reconstruction process.

IR has seen a very rapid introduction into CT clinical practice in recent years, primarily due to the increased focus on radiation dose optimization. Siemens Healthineers, focus in particular has been to provide the necessary technological tools for achieving the right dose for the right diagnostic task. This focus is aligned with the ALARA principle – to use As Low As Reasonably Achievable radiation dose to warrant a diagnostic image quality. It is well known that a trade off of dose reduction is a degradation in image quality, most notably an increase in image noise. The first IR technology commercially developed by Siemens Healthineers for CT was the Iterative Reconstruction in Image Space (IRIS). IRIS directly addressed the problem of increased image noise in reduced dose acquisitions. IRIS is a scientifically validated technology that is effective in reducing image noise in a variety of clinical applications.

However, IR technologies should not only aid noise reduction but also reduce image artifacts: These can be exacerbated when using reduced dose CT acquisitions or fast acquisition techniques. As response to this, the next IR technology developed by Siemens Healthineers was the Sinogram Affirmed Iterative Reconstruction (SAFIRE), launched in 2010. SAFIRE was Siemens Healthineers, first IR technology to integrate a correction loop into the raw-data domain (also called 'sinogram') and to add a model of the CT system geometry during the data forward projection. This correction loop that operates back to the sinogram domain is particularly helpful for reducing artifacts. In SAFIRE, a second correction loop in image space is applied iteratively to reduce image noise. SAFIRE has been used extensively since its introduction, and a wealth of scientific literature has consistently supported the benefits of SAFIRE for dose reduction while maintaining high image quality in applications ranging from routine to specialized body and neuro CT, in both adults and pediatrics.

One of the current challenges in the widespread use of IR technology has been the potential changes to the image texture when an IR algorithm is operated to aggressively reduce image noise. As a result, only a limited number of clinical applications may benefit from the advantages of the higher noise reduction, hence somewhat reducing its full potential for radiation dose reduction. Image texture refers to the typical appearance (or distribution) of the image noise in CT images, which, when affected drastically, may produce an over-smooth look that is sometimes referred to anecdotally as a 'plastic' or 'blotchy' look. These effects are typically more noticeable when IR is applied to reconstruct thicker slices (e.g., 5 mm) or in applications where for the clinical task the low-contrast detectability is important, hence limiting the full range of radiation dose reduction potential.

ADMIRE

To address the emerging challenges in CT reconstruction, Siemens Healthineers has now released a new state-of-the art IR technology called ADMIRE: advanced modeled iterative reconstruction (Figure 11). ADMIRE belongs to the category of statistical IR methods, which also denote model-based iterative reconstruction. As with other implementations of statistical IR methods, ADMIRE is characterized by (i) the use statistical weighting in the raw-data space followed by a back projection (unfiltered or filtered), (ii) the application of a regularization function consisting in a statistical model in the image space, and (iii) the use of forward projection (aka data re-projection) with an adequate CT system model. The latter forward projection step generates pseudo raw data which is compared to the measured raw data, i.e. subtracted, and reinserted into the loop afterwards (see loop A in Figure 11). The process of repetitively comparing the measured raw data with pseudo raw data contributes primarily to the cancellation of artifacts, and to a lesser extent to noise reduction, which is mainly reduced by loop B which contains the regularization function in the image space.

It should be noted that repetition of the forward projection operation (loop A) is often the most demanding computationally, and hence traditional SIR methods typically require hours of reconstruction time, which noticeably limits their application to routine clinical workflow. To achieve efficient speeds, ADMIRE uses innovative mathematical formulations that allow a reduction in the number of computationally heavy forward projection operations; hence, few iterations are needed for statistical optimization.

The original comparison of pseudo raw data with measured raw data turns into a comparison of the current image data set with a master 3D volume that can be visualized as an WFBP reconstruction utilizing a special preconditioning filter which propagates the statistically relevant information into the image domain. Although the regularization function thereby becomes more sophisticated, the effective iteration speed is substantially higher, since only a few iterations are needed. Therefore the ADMIRE reconstruction starts with a limited number of iterations in loop A (Figure 11), which are targeted to remove geometric imperfections such as cone-beam artifacts as well as streak artifacts using the statistical weighting in the raw data space.

Subsequently, iterations in the image space, loop B (see Fig. 11), are performed to finalize the statistical optimization, i.e. reaching a target noise reduction level that is determined by the selected ADMIRE strength.

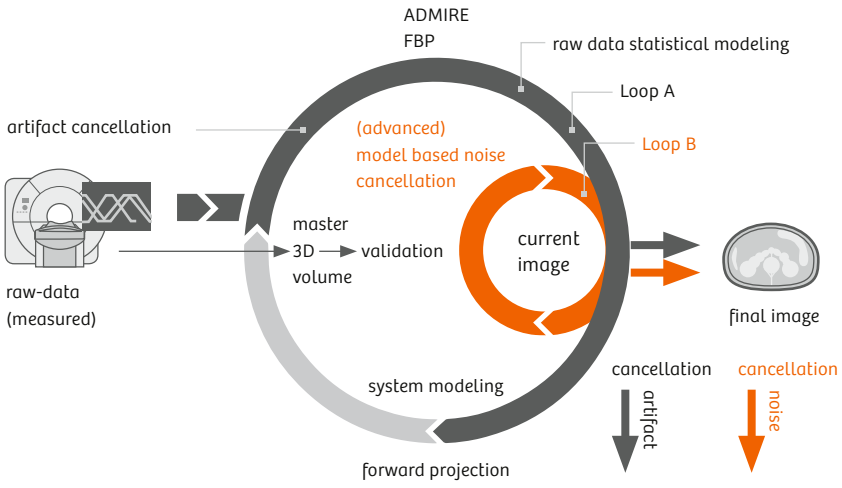

Figure 11: Algorithm scheme of ADMIRE.

Fundamentals of ADMIRE in three steps:

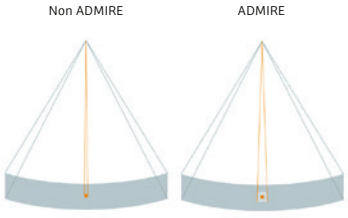

Improvement of quality in every projection and measuring points based on information of neighbor detector elements for removing streak artifacts.

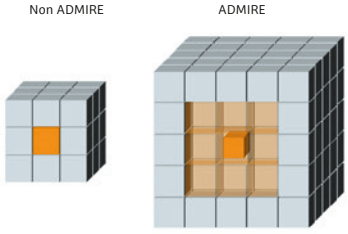

Analysis on a large scale in all directions to distinguish anatomical structures from noise. This results in a natural image impression and excellent IQ.

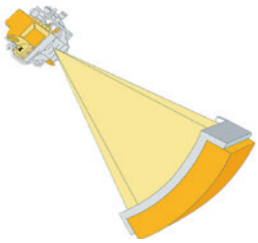

1. ADMIRE uses an advanced statistical weighting of all projections in the raw-data space. As a result, each projection recorded by individual detector elements is weighted according to its statistical quality (e.g., noisy vs higher quality signal), and takes into account the information of neighbor detector elements. This contributes to image noise reduction and notably to streak artifact reduction.

2. Advanced regularization intelligently separates noise from actual anatomical structures in the imag e. Further, ADMIRE operates within a larger 3D voxel neighborhood. These characteristics contribute to an improved capability for dose reduction through the enhancement of noise reduction and because the natural 'texture appearance' of the CT images is maintained even at higher ADMIRE strengths and/or thicker image slices.

3. ADMIRE incorporates a more complete modeling of the CT geometry and scanner components and characteristics such as detector type and size (e.g., Stellar and Stellar^{Infinity} detectors) and flying focal spot. This contributes to improved spatial resolution and the reduction of cone-beam artifacts.

Practical Aspects and Clinical Use

ADMIRE has five adjustable strength levels which can be optimized according to the clinical application and radiologist's preference. The strength level, which can be selected between 1 and 5, controls the amount of noise reduction; the highest amount of noise reduction is achieved with strength 5, and strength 3 is offered as the default value. ADMIRE has the advantage that the user can select a priori the spatial resolution, which is maintained regardless of the strength level chosen. Figure 12 shows an example of a coronary CT angiography in which the same CT data was reconstructed with conventional WFBP and with ADMIRE using strength levels 3, 4, and 5. In all cases, the anatomical borders are maintained with excellent delineation of the edges indicating preservation of spatial resolution, while at the same time the image noise substantially decreases as the ADMIRE strength level increases from 3 to 5.

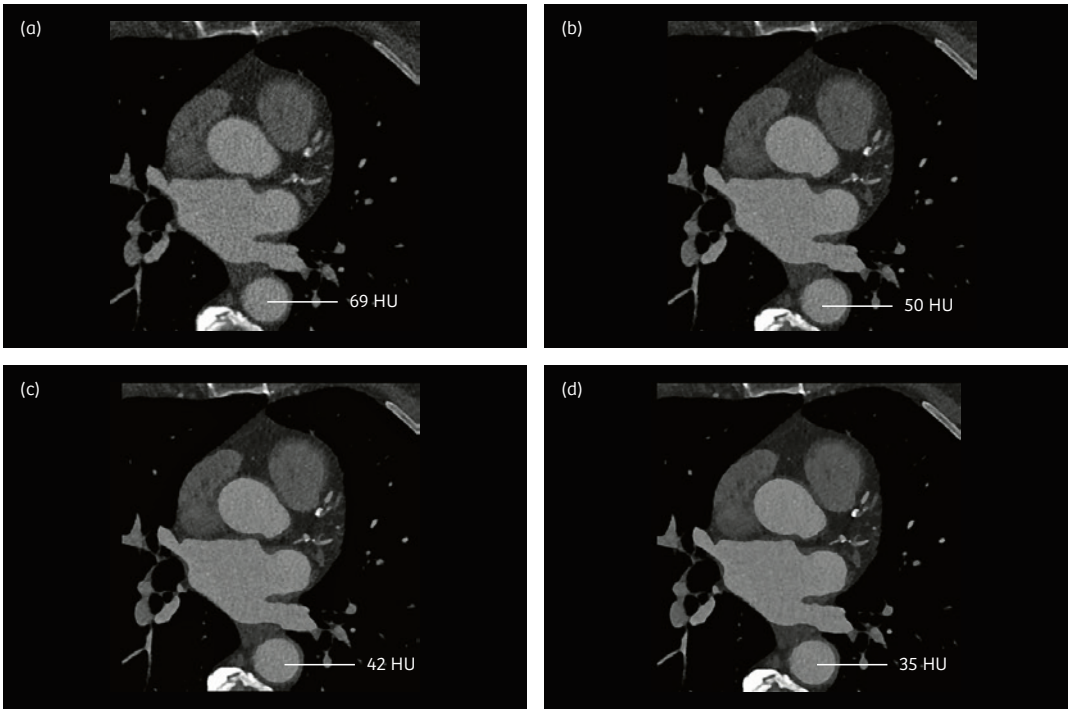

Figure 12: Example of ADMIRE in cardiac CT angiography. Patient was scanned with 70 kVp and 555 mAs, with recorded radiation exposure parameters of $CTDI_{vol}$ = 1.56 mGy, DLP = 26.1 mGy cm. Images were reconstructed with 0.5 mm thickness using (a) WFBP, (b) ADMIRE strength 3, (c) ADMIRE strength 4, and (d) ADMIRE strength 5. The images illustrate the continuous decrease in image noise as a function of ADMIRE strength.
Courtesy of The Medical University of South Carolina, USA.

The full benefits of ADMIRE for noise reduction, spatial resolution improvement and artifact reduction are best achieved with the concurrent use of the Stellar^{Infinity} and Stellar CT detectors; This is available in SOMATOM Force and selected CT scanners from the SOMATOM Definition family such as the Edge and Flash scanners. Figures 13 and 14 show examples of the excellent performance of ADMIRE. They show low contrast detectability and spatial resolution for neuro CT applications such as routine non-enhanced head CT and temporal bone imaging respectively. Figure 15 shows an example of streak artifact reduction with ADMIRE for a CT scan using a fast acquisition technique (Turbo Flash) and a tube potential of only 70 kVp ($CTDI_{vol}$ = 1.67 mGy, DLP = 82 mGy cm). Artifact reduction for this example can be mainly attributed to ADMIRE's use of statistical weighting in the raw-data space.

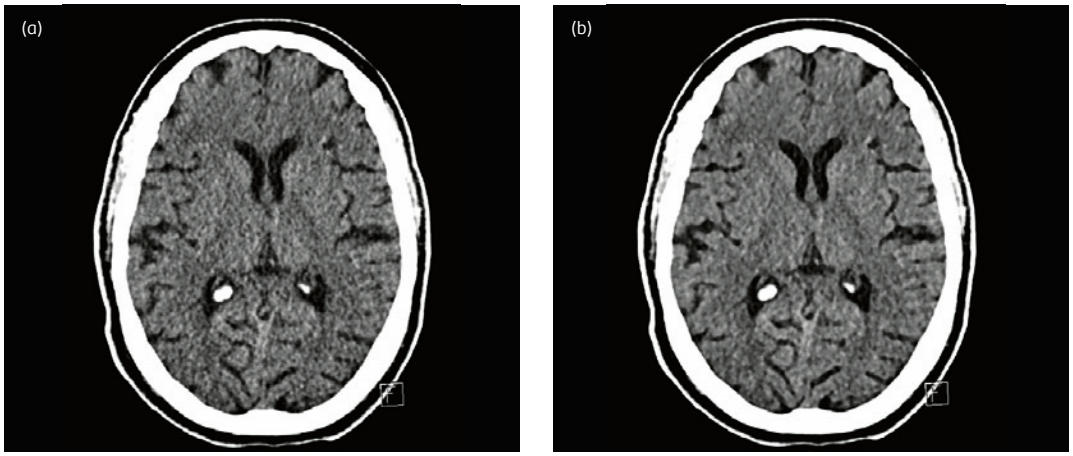

Figure 13: Example of routine non-enhanced head CT using a thin slice (1.0 mm) reconstruction. (a) routine WFBP, and (b) ADMIRE with strength 3. Courtesy of The Medical University of South Carolina, USA.

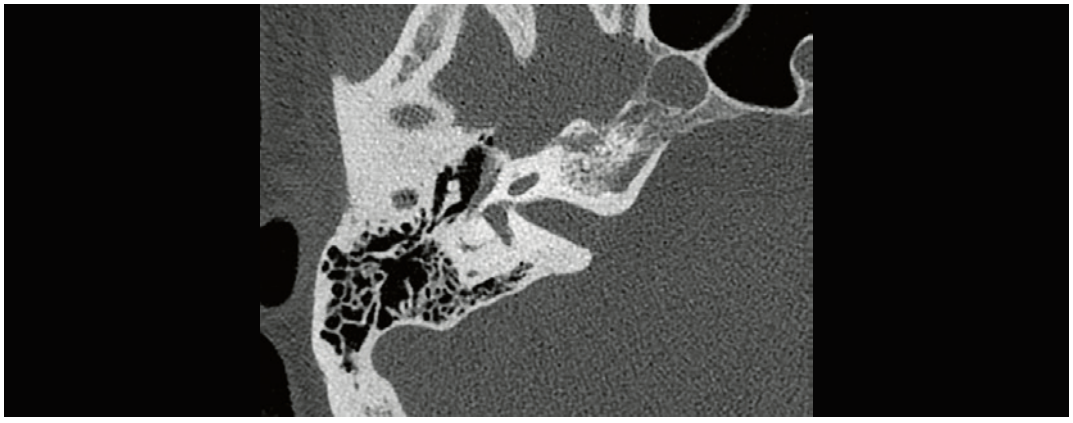

Figure 14: ADMIRE use with an ultra-high resolution temporal bone protocol for imaging of the inner ear, with an effective slice thickness of 0.4 mm. Courtesy of University Medical Center of Mannheim, Germany.

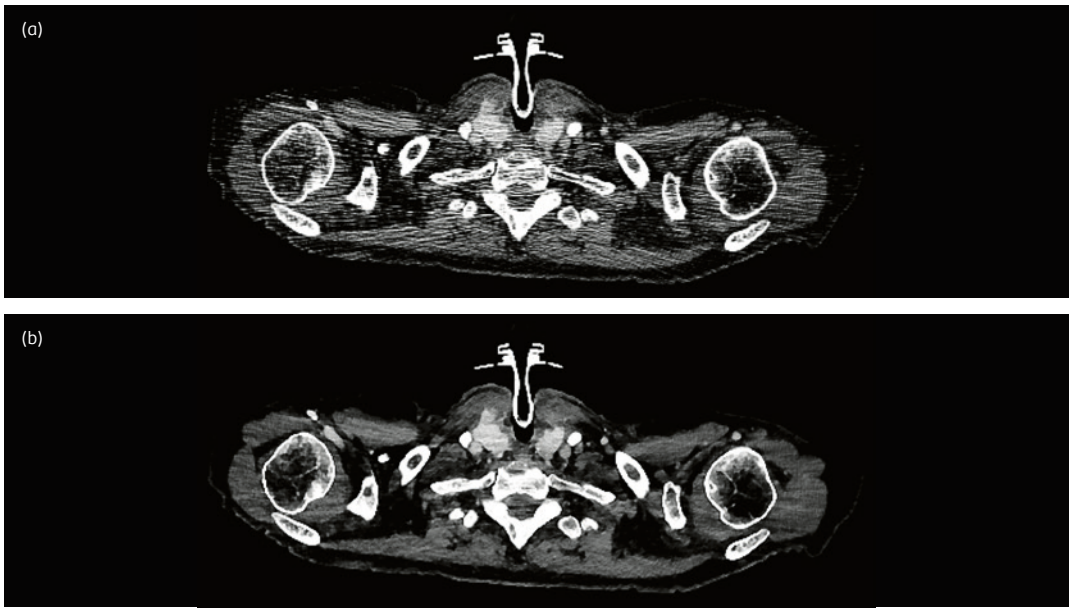

Figure 15: Artifact reduction with ADMIRE in highly attenuating anatomy such as the shoulders for an examination using 70 kVp (a) WFBP, and (B) ADMIRE. Courtesy of University Medical Center of Mannheim, Germany.

ADMIRE is compatible with dual energy CT, a technique that continues to gain importance in clinical practice. Figure 16 provides an example of contrast-enhanced dual energy CT acquisition of the abdomen using a tube potential pair of 100/150 Sn kV. Excellent image quality is achieved for both the conventional mixed image as well as for the virtual-non contrast image that used ADMIRE.

ADMIRE also works synergistically with the Tin Filter, a state-of-the art technology available in SOMATOM Force that enables 'ultra-low' dose acquisitions for non-enhanced CT examinations such as chest CT. Figure 17 shows an example of a patient undergoing two consecutive unenhanced CT scans of the chest. The first scan used a routine protocol at 120 kVp and was reconstructed with WFBP, while the second scan used 100 kVp with Tin Filter and ADMIRE reconstruction. Remarkably, the scan with Tin Filter and ADMIRE required a scanner radiation output which was only 8% of that of the routine acquisition (0.34 vs 4.27 mGy, respectively); yet image quality was comparable.

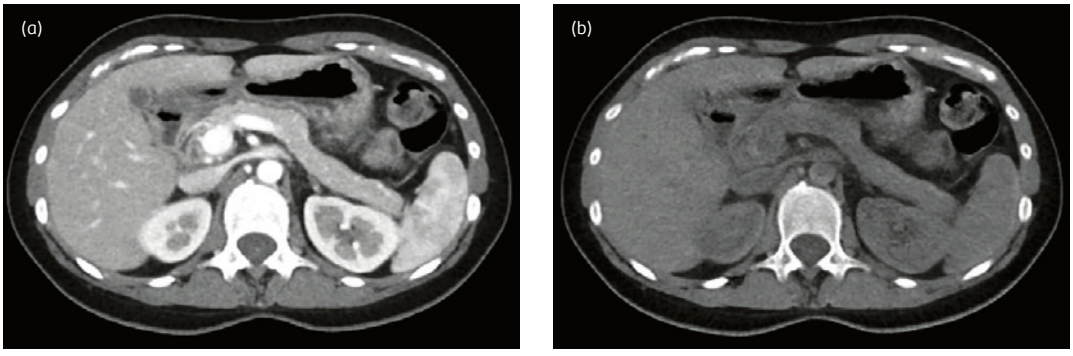

Figure 16: Application of ADMIRE in Dual Energy imaging. Data was acquired using 100/150 Sn. Images were reconstructed using ADMIRE strength 3 and were used to generate (a) mixed image and (b) virtual-non contrast image series. Courtesy of The Medical University of South Carolina, USA.

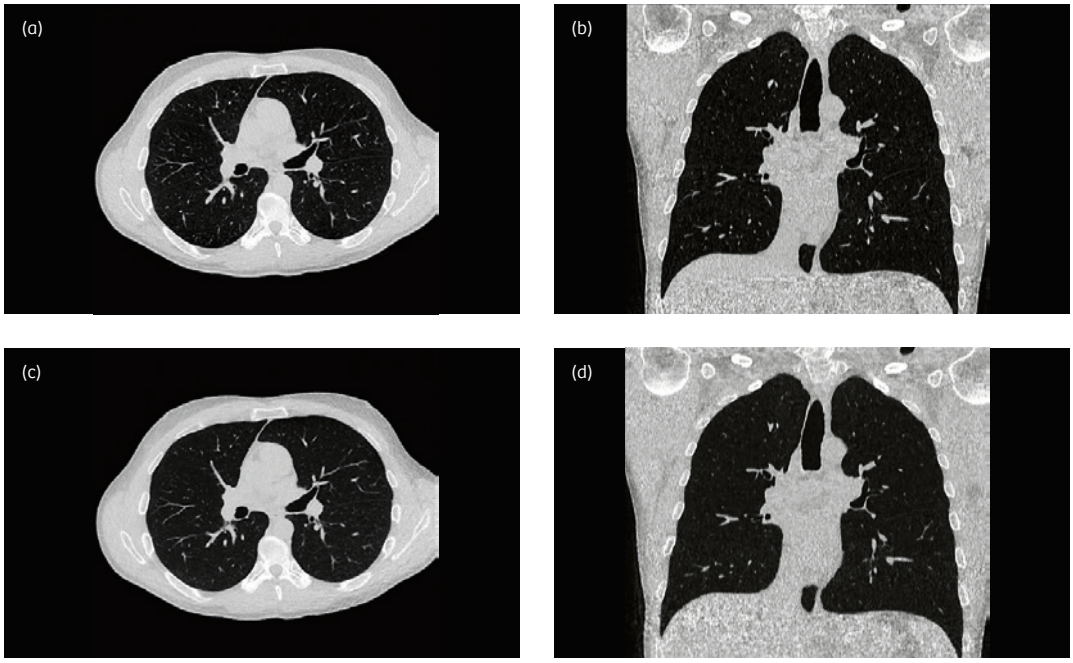

Figure 17: The example depicts images of a young patient who underwent a routine chest CT protocol at 120 kVp ($CTDI_{vol}$ = 4.27 mGy, DLP = 171 mGy cm) reconstructed with conventional WFBP (a, b). Below (c, d) are shown results obatined by a reduced dose chest CT protocol with 100 kVp and Tin Filter reconstructed with ADMIRE strength 4 ($CTDI_{vol}$ = 0.34 mGy, DLP = 13.6 mGy cm). Courtesy of the Mayo Foundation, USA.

Within recent years after its introduction in December 2013, ADMIRE has created significant interest as demonstrated by publications in peer-reviewed scientific literature. Table 1 lists some of the publications which cover a variety of clinical applications (chest, abdomen, cardiac, and neuro CT) and which highlight technological advances of ADMIRE for dose reduction, noise reduction, texture preservation, and improvement of spatial resolution.

Publication	Study Conclusion	Aspects of ADMIRE investigated [Clinical Application]
Gassenmaier et al. [2014]	Use of third-generation Dual Source CT enables stent lumen visibility of up to 80% in metal stents and 100% in bioresorbable stents.	Spatial resolution, dose and noise reduction **[cardiac CT]**
Gordic S et al. [2014]	The study suggests that chest CT for the detection of pulmonary nodules can be performed with third-generation dual-source CT producing high image quality, sensitivity, and diagnostic confidence at a very low effective radiation dose of 0.06 mSv when using a single-energy protocol at 100 kVp with spectral shaping and when using advanced iterative reconstruction techniques.	Dose reduction, noise reduction **[low-dose chest CT]**
Gordic S et al. [2014]	Abdominal CT using ADMIRE results in an improved image quality with lower image noise as compared with FBP, while the ttenuation of various anatomical regions remains constant among reconstruction algorithms.	Noise reduction, texture preservation **[abdomen CT]**
Meyer M et al. [2015]	Temporal bone imaging without z-axis-UHR filter and a novel third generation IR algorithm allows for significantly higher image quality while lowering effective dose when compared to the first two generations of Dual Source CTs.	Spatial resolution, noise and dose reduction **[neuro CT]**
Newell JD et al. [2015]	The third-generation Dual Source CT scanners using third generation iterative reconstruction methods can acquire accurate quantitative CT images with acceptable image noise at very low-dose levels (0.15 mGy). This opens up new diagnostic and research opportunities in CT phenotyping of the lung for developing new treatments and increased understanding of pulmonary disease.	Dose reduction, noise reduction, **[low-dose chest CT]**
Rompel et al. [2016]	The third-generation DSCT at 70 kVp provided good objective and subjective image quality at lower radiation exposure. ADMIRE improved objective and subjective image quality.	Dose, image quality **[pediatric CT]**
Schaller F et al. [2016]	ADMIRE is able to reduce image noise considerably (up to 50%) without any obvious negative imapact on lesion depiction as assessed visually. Noise reduction of ADMIRE seems to be independent of slice thickness.	Noise reduction, image quality **[abdomen CT]**
Scholtz JE et al. [2015]	Contrast-enhanced 90 kVp neck CT is feasible, and ADMIRE 5 shows superior objective image quality compared with filtered back projection. ADMIRE 3 and 5 show the best subjective image quality.	Image quality **[neck CT]**
Solomon J et al. [2015]	Low-contrast detectability performance increased with increasing object size, object contrast, dose, slice thickness, and ADMIRE strength. Compared to FBP, ADMIRE allows a substantial radiation dose reduction while preserving low-contrast detectability.	Image quality **[neuro CT]**
Wenz H et al. [2015]	Combination of third-generation DSCT spiral cCT with an advanced model IR technique significantly improves subjective and objective image quality compared to standard sequential cCT acquisition acquired at identical dose levels.	Low-contrast detectability, dose reduction **[body CT]**

Table 1: Summary of selected scientific publications of ADMIRE for various clinical applications.

Conclusion

Compared with previous iterative reconstruction approaches, ADMIRE has the potential to

- result in a higher noise reduction performance and improved low-contrast detectability. This is combined with a well-maintained noise texture of the reconstructed images, which closely resembles the familiar FBP-like noise impression (see Figs 18 and 19). Note that ADMIRE also provides significant noise reduction at improved low-contrast detectability for thicker slice widths such as 3 mm or 5 mm.
- achieve an efficient reduction of streak artifacts and substantial image noise in low-dose datasets and object regions with strongly non-isotropic CT attenuation (e.g., in the shoulder region), see Figs 20 and 21.
- allow for improved resolution at high-contrast edges in the image compared with images reconstructed with FBP, see Fig. 22.

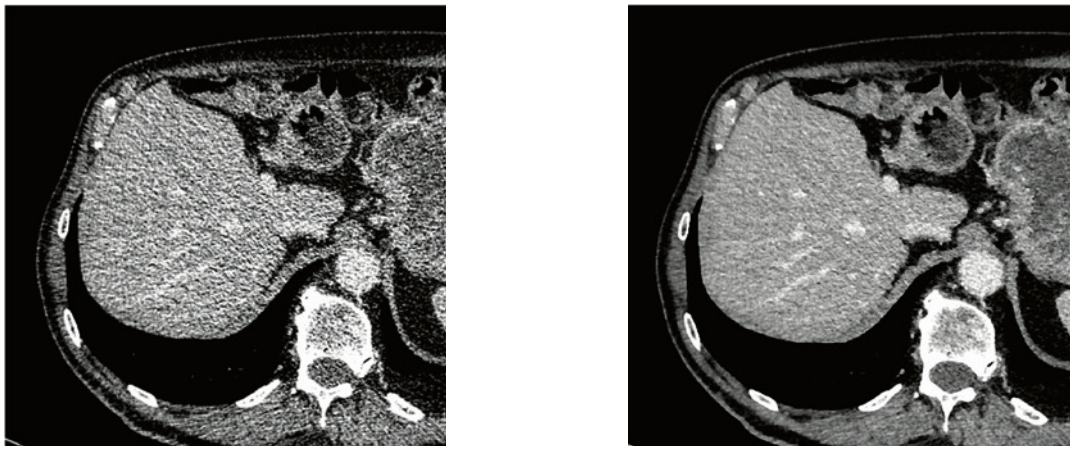

Figure 18: Clinical liver image reconstructed with WFBP (left) and ADMIRE strength 5 (right). Note the significant noise reduction without loss of spatial resolution at a well-maintained image noise texture.

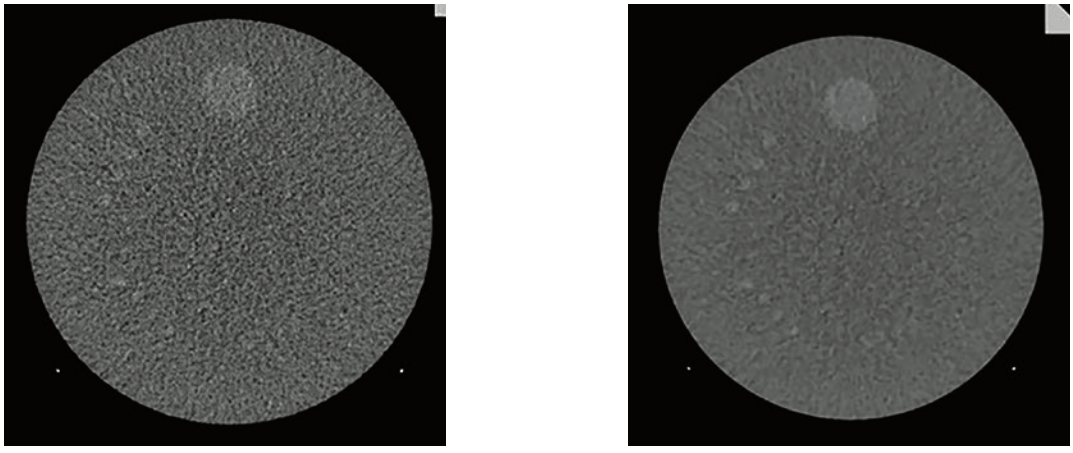

Figure 19: Low-contrast module of the ACR accreditation phantom, reconstructed with FBP (left) and with ADMIRE strength 5 (right). Image noise is reduced and low-contrast detectability is improved – note the 4 small cylinders on the bottom left which are barely visible on the FBP image. Courtesy of the Clinical Innovation Center, Mayo Clinic Rochester, Minnesota, USA.

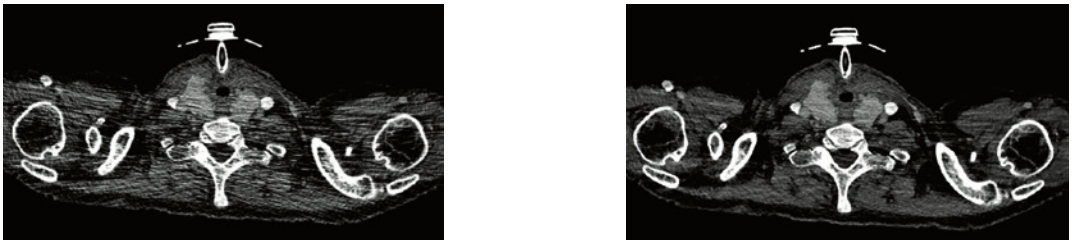

Figure 20: Clinical shoulder image reconstructed with WFBP (left) and with ADMIRE strength 3 (right). Note the significant reduction of streak artifacts with ADMIRE.

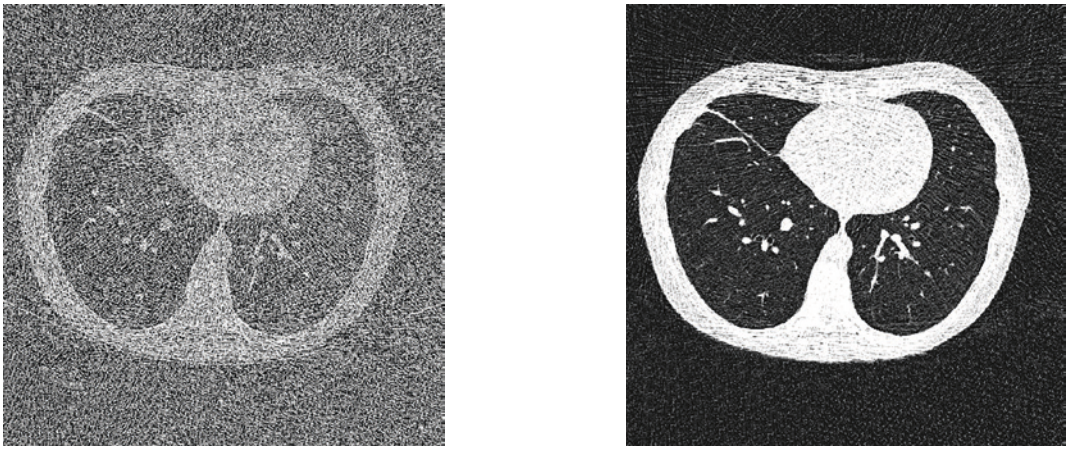

Figure 21: Clinical lung image at an extremely low dose ($CTDI_{vol}$ = 0.04 mGy, DLP = 1.4 mGy cm) reconstructed with WFBP (left) and with ADMIRE strength 5 (right). This example illustrates the potential of ADMIRE to substantially reduce image noise in CT images acquired at every low radiation dose.

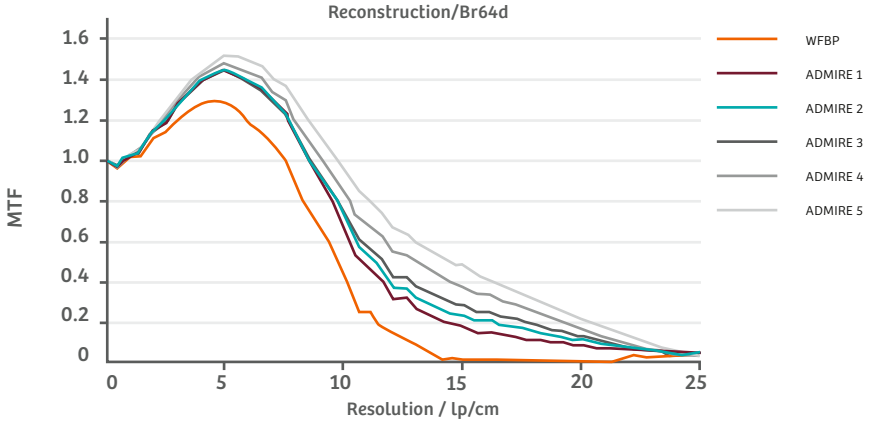

Figure 22: In-plane modulation transfer function of the sharp body kernel Br64, measured using a small high-contrast object and reconstructed with filtered back projection (WFBP) and different strength settings of ADMIRE (1–5). As the ADMIRE strength setting increases, so does the spatial resolution (Gordic et al., 2014).

2. Increased spatial resolution for enhanced detail visualization in CT angiography, bone and inner ear imaging

SOMATOM Force significantly improves spatial resolution in clinical routine imaging due to the following factors: data acquisition using the small focal spot of the Vectron X-ray tube with a power-independent focal spot size; excellent in-plane and through-plane sampling thanks to the small detector apertures of the Stellar^{Infinity} detector in combination with the in-plane and z-axis flying focal spot; and ADMIRE iterative reconstruction. In scan modes with very fast gantry rotation, for example 0.25 s, a diagonal flying focal spot is used to combine the benefits of both in-plane and z-axis oversampling through periodic focal spot movement. Increased spatial resolution may be beneficial in CT angiographic studies, in particular for the visualization of very small vessels such as the coronary arteries. A known limitation in cardiac CT is the presence of significant coronary artery calcification, and the capacity to reliably evaluate the in-stent lumen in smaller coronary stents (Andre et al., 2013; Maintz et al., 2009). Maintz et al. evaluated 29 commonly used coronary stents using DSCT (SOMATOM Definition) and found an average lumen visualization of 54 ± 8.3%. Andre et al. compared the performance of DSCT (SOMATOM Definition) with 256-MSCT with wider detector coverage for the in vitro assessment of stent lumen diameters. DSCT and 256-MSCT revealed similar stent lumen diameters (50.7 ± 7.2% vs. 50.8 ± 7.4%, p = 0.98). According to the authors, only stents with a diameter > 3 mm allowed for a sufficient stent lumen assessment in both scanners and showed a relative lumen diameter of 60–66%. Researchers from the Institute of Diagnostic Radiology, Würzburg University, Germany (T. Gassenmaier, N Petri, W. Voelker and T. Bley) scanned the 29 coronary stents with different diameters (2–4 mm) already evaluated (Maintz et al., 2009) on SOMATOM Force. The results, shown in Figures 21 and 22, demonstrate a significant improvement in the visualization of the in-stent lumen using SOMATOM Force. The authors conclude that “the use of third-generation Dual Source CT scanners enables stent lumen visibility of up to 80% in stents with 3 mm diameter and may therefore be a valid method for detecting in-stent restenosis” (submitted for publication).

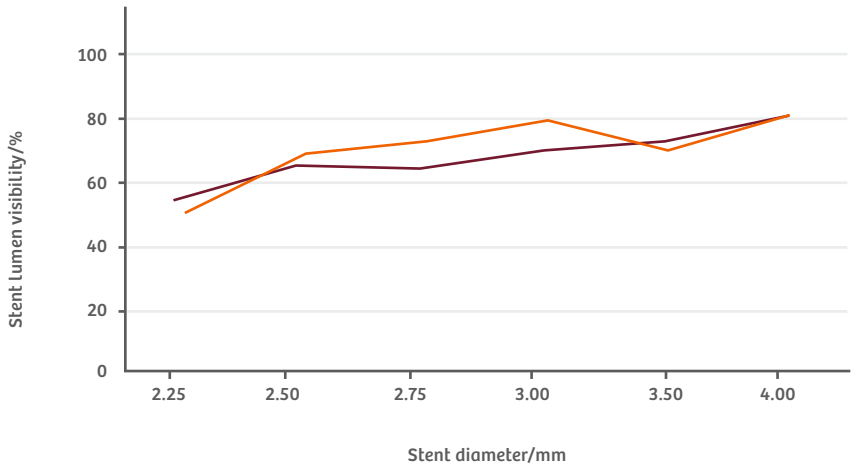

Figure 23: Coronary stents scanned on SOMATOM Force. Influence of stent diameter on lumen visibility, Bv59 kernel, ADMIRE strength 4. Courtesy of the Institute of Diagnostic Radiology, Würzburg University, Germany.

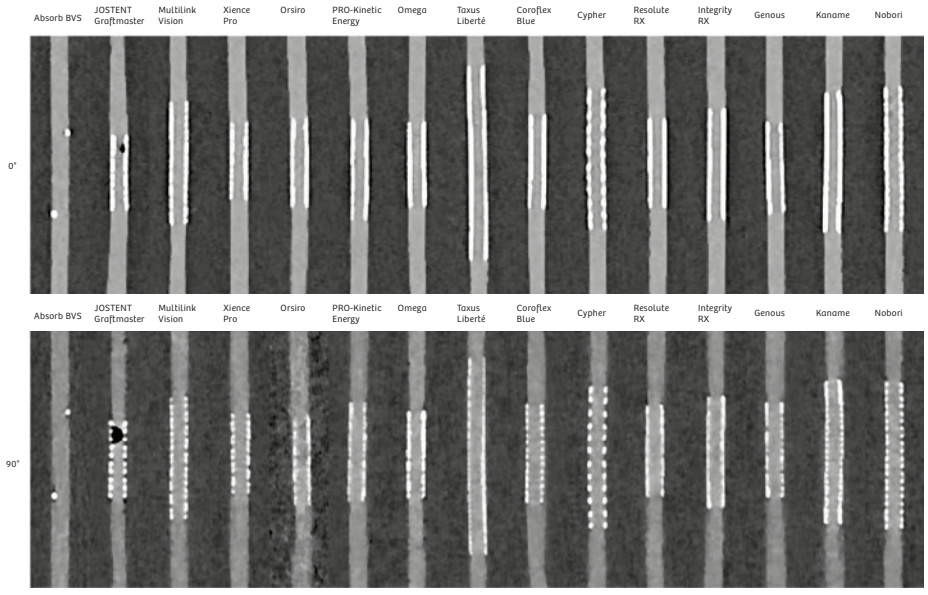

Figure 24: Three-millimeter coronary stents scanned on SOMATOM Force. Longitudinal multiplanar reformations of all stents with a diameter of 3.0 mm at 0° and 90° to the z-axis using the Bv59 kernel, ADMIRE strength 4. Courtesy of the Institute of Diagnostic Radiology, Würzburg University, Germany.

Figure 25 is a clinical example illustrating the potential of high resolution coronary CTA to increase diagnostic confidence when coronary calcifications are present. Using standard CT technology, a high-grade stenosis of the diagonal branch of the left coronary artery (LAD) was suspected. The follow-up scan with SOMATOM Force revealed no significant stenosis.

Conventional CT

SOMATOM Force –
ADMIRE strength level 4

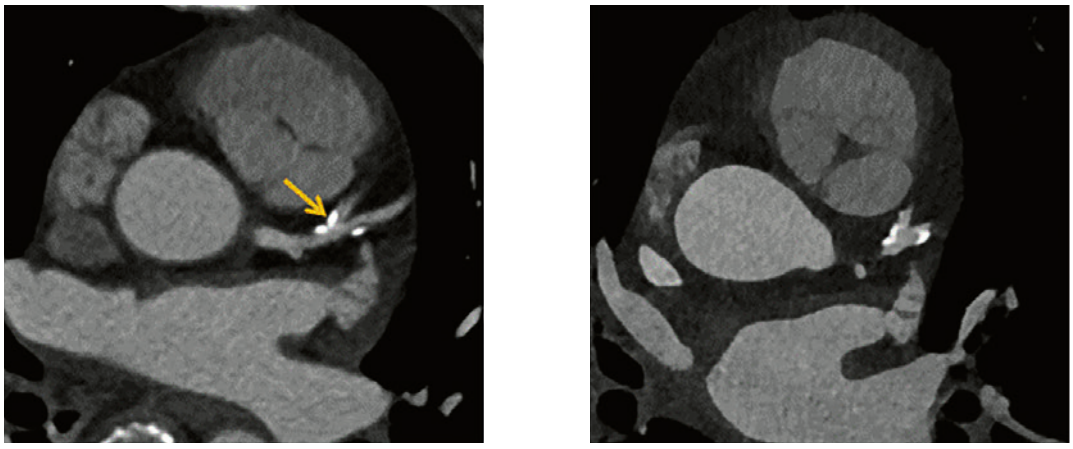

Figure 25: Follow-up examination of a patient for coronary artery disease. Left: Conventional CT indicates severe stenosis of the diagonal branch of the left ascending coronary artery (yellow arrow). Right: Follow-up examination on a SOMATOM Force excludes significant stenosis. Courtesy of University Hospital Zurich, Switzerland.

Another area that benefits from an increase in spatial resolution is inner ear and bone imaging. SOMATOM Force offers unparalleled spatial resolution for clinical imaging due to an in-plane resolution of 26 lp/cm (see Fig. 5) at a MTF cutoff frequency of 32 lp/cm in ultra-high resolution (UHR) mode and the thinnest reconstruction slice width of 0.4 mm. Researchers from the Institute of Diagnostic Radiology at Mannheim University, Germany, have evaluated the image quality and radiation dose of inner ear imaging with SOMATOM Force and compared the results with those of previous generations of high-end CT systems (submitted for publication). They conclude that SOMATOM Force offers a significantly higher subjective and objective image quality than previous technologies. In addition, the total effective radiation dose was up to 63% lower. According to the authors, the mean dose length product for inner ear imaging decreased from 219.3 mGy cm in 2004 (SOMATOM Definition) to 134.1 mGy cm in 2009 (SOMATOM Definition Flash), and then to 83.8 mGy cm in 2013 (SOMATOM Force). At the same time, the signal-to-noise ratio (SNR) of the calvaria increased from 4.15 to 12.97, see Figures 26 and 27 (submitted for publication).

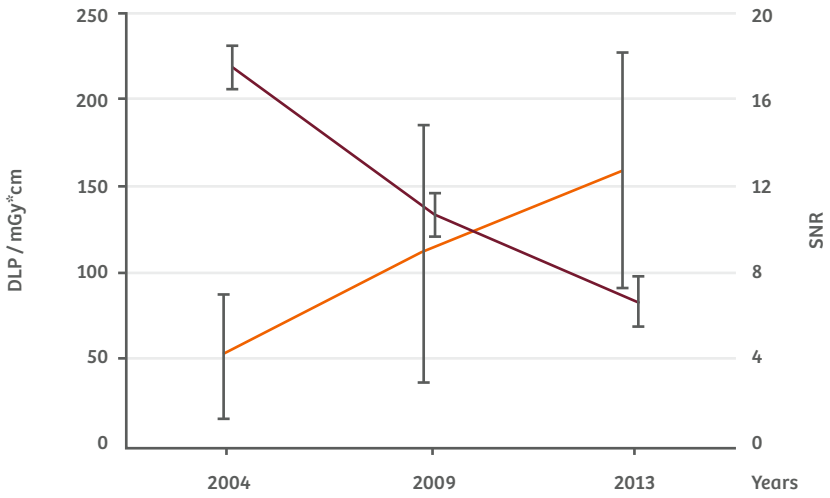

Figure 26: Dose length product (light blue line [DLP]) and signal-to-noise ratio (dark blue line [SNR]) of the calvaria plotted against the different generations of high-end CT systems at their first introduction in 2004 (SOMATOM Definition), in 2009 (SOMATOM Definition Flash), and in 2013 (SOMATOM Force).
Courtesy of Institute of Diagnostic Radiology, Mannheim University, Germany.

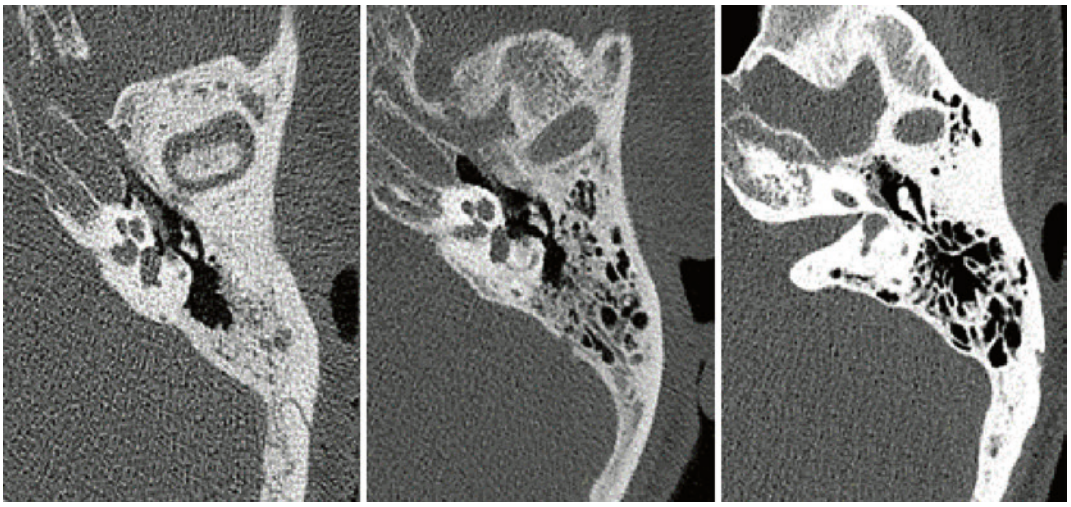

2004 2009 SOMATOM Force 2013

Figure 27: Typical inner ear images from three generations of high-end CT systems.
Courtesy of Institute of Diagnostic Radiology, Mannheim University, Germany.

3. Fast scan speed with high temporal resolution for cardiac CT, CT angiography, pediatric CT, and the management of un-cooperative patients

In dual source high-pitch spiral scan mode (Turbo Flash spiral, for a technical description see Flohr et al., 2009), SOMATOM Force can operate at a maximum scan speed of 737 mm/s (0.25 s rotation, pitch 3.2) with 66 ms temporal resolution per image. This scan technique achieves very fast volume coverage and a total scan time of well below second for most anatomical regions. It is therefore potentially beneficial in pediatric CT and for managing patients with a limited ability to co-operate, such as trauma cases. Thanks to the very high scan speed and a temporal resolution of 66 ms per image, the sedation of children can potentially be avoided (Hagelstein et al., 2015), and CT scans can be performed during free breathing.

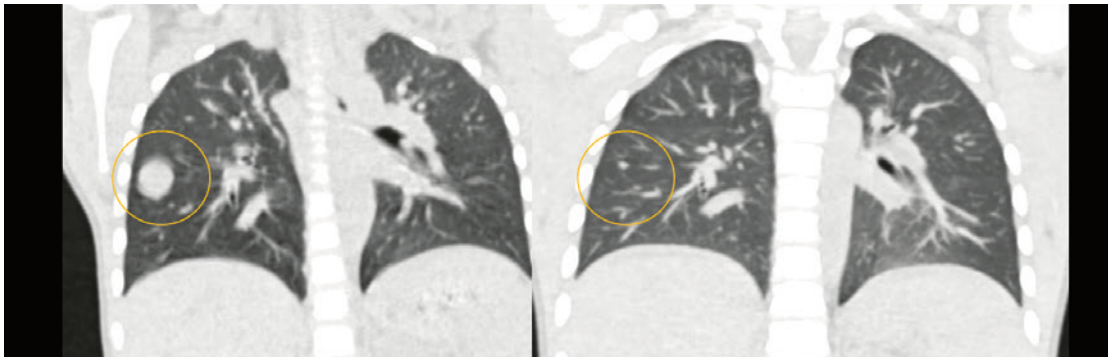

Figure 28: Follow-up study of a 5-year-old patient with neuroblastoma and lung metastasis. Left: Standard thorax CT. Right: Turbo Flash thorax CT without patient sedation, scan time 0.3 s, radiation dose 0.4 mSv.
Courtesy of the Institute of Diagnostic Radiology, Mannheim University, Germany.

Turbo Flash spiral can be combined with ECG-triggering for cardiac CT imaging, covering the entire heart (~120 mm scan range) within one heartbeat in the mid- to end-diastolic phase (scan time ~170 ms) at 66 ms temporal resolution per image. The ECG-triggered Turbo Flash spiral does not acquire redundant scan data, but rather the very minimum amount of data needed for image reconstruction (see Flohr et al., 2009). It is therefore a dose-efficient scan mode and enables coronary CTA at very low radiation doses such as 0.44 mSv (Meyer et al., 2014) that cannot be achieved using other scan techniques. Due to the high scan speed of 737 mm/s, Turbo Flash spiral is clinically robust for ECG-triggered cardiac imaging in patients with heart rates of up to 70–75 bpm. This heart rate limit is well known and clinically accepted in cardiac imaging with single source CT.

Meanwhile, several authors have investigated coronary CTA with Turbo Flash spiral on SOMATOM Force. Morsbach et al. (Morsbach, 2014) evaluated the image quality, the maximum heart rate with diagnostic image quality, and the radiation dose of Turbo Flash high-pitch dual source coronary CTA, with a cardiac motion phantom and in 20 consecutive patients. The authors conclude that Turbo Flash high-pitch coronary CTA provides diagnostic image quality for heart rates up to 73 bpm (see Fig. 29), at an average radiation dose of 0.6 mSv.

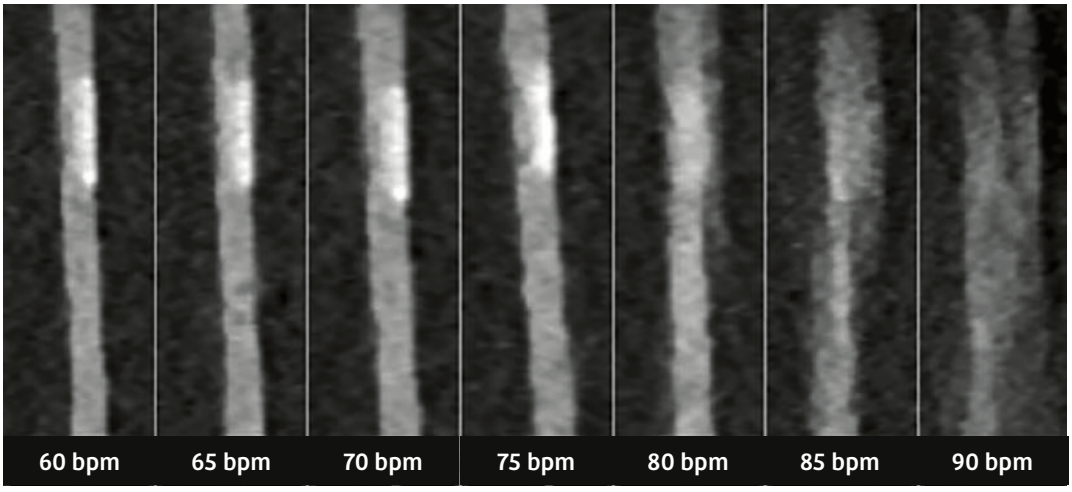

Figure 29: Image quality examples of contrast-medium-filled tubes with calcified plaque at different simulated heart rates. Image quality is excellent to good (scores 1 and 2) for heart rates ≤ 75 bpm. (Morsbach et al., 2014)

Gordic et al. (Gordic, 2014) defined the average heart rate (HR) and heart rate variability (HRV) required for diagnostic imaging of the coronary arteries in 50 consecutive patients undergoing prospectively ECG-triggered high-pitch CTA using third-generation DSCT. No beta-blockers were admitted in this study. According to Gordic et al., "high-pitch CTA performed with a third-generation 192-slice Dual Source CT system yields diagnostic image quality of the coronary arteries in patients with an average HR up to 70 bpm. At HR between 70 and 75 bpm, studies were diagnostic in 88%. In contrast to the average HR, HRV was not significantly related to the image quality of the coronary arteries. The high-pitch data acquisition of the heart is fast, taking less than 0.2 s, and is associated with low radiation dose of 0.4 mSv."

Fig. 30 illustrates the image quality that can be achieved with ECG-triggered Turbo Flash high-pitch coronary CTA.

In a cross-sectional, international, multicenter study (Protection I (Hausleiter et al., 2009) with 50 study sites (21 university hospitals and 29 community hospitals), the estimated radiation dose in 1,965 patients undergoing coronary CTA between February and December in 2007 was evaluated. At that time, the median estimated radiation dose for coronary CTA was 12 mSv, with a high variability between 5.7 mSv and 36.5 mSv. Using an X-ray tube voltage of 100 kV instead of 120 kV lowered the radiation dose by 31% (Protection II, (Hausleiter et al., 2010)) to an estimated value of 8.4 mSv. Finally, using ECG-triggered axial scanning instead of ECG-gated spiral CT, the radiation dose was further reduced to an average of 3.5 mSv (Protection III, (Hausleiter et al., 2012)). In light of the radiation dose values in clinical practice today, an average radiation dose of 0.5 mSv for a coronary CTA with Turbo Flash spiral in combination with low-kV imaging (see section 4) may create new potential and open up new applications for cardiac CT imaging.

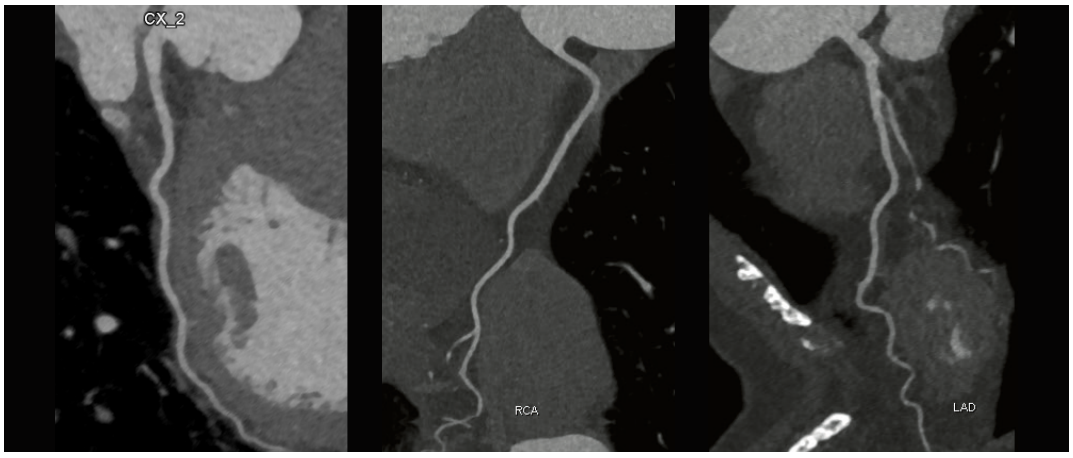

Figure 30: ECG-triggered Turbo Flash high-pitch coronary CT angiography for rule-out of coronary artery disease in a regular adult (HR: 56 bpm) with a BMI of 24 and a scan range of 142 mm. Low-kV imaging with 70 kV and fast acquisition within 0.2 s results in a dose as low as 0.09 mSv. Courtesy of Adventist Hospital Sydney, Australia.

The ECG-triggered Turbo Flash spiral has also often been used to perform very fast thoraco-abdominal CT angiographic (CTA) studies at a very low radiation dose, covering a scan range from the aortic arch to the iliac arteries, and with the diagnostic image quality of the coronary arteries, e.g., for TAVI (TAVR) planning. Fig. 31 shows a clinical example of a Turbo Flash CTA in a patient with an abdominal aortic stent graft.

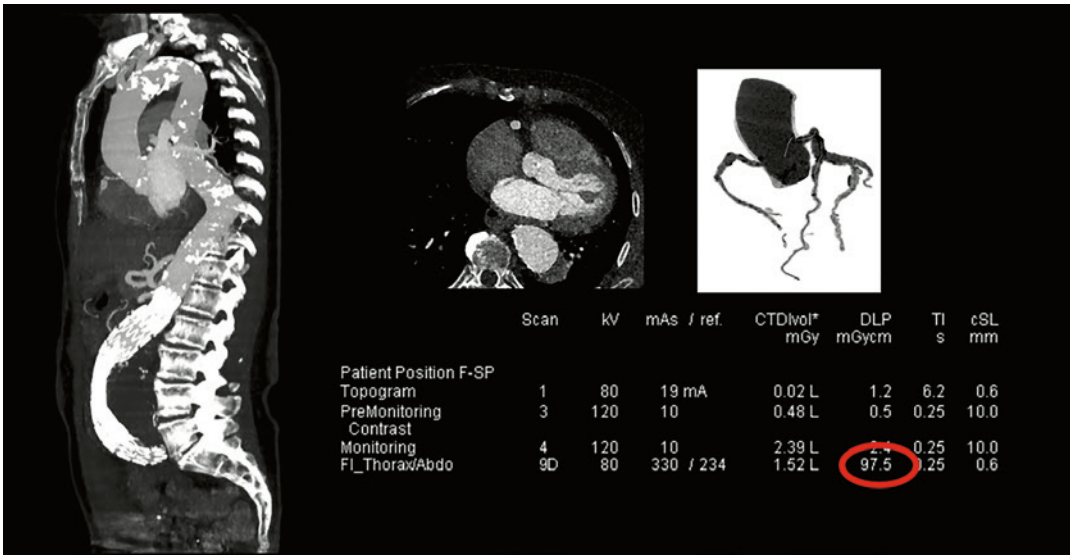

Figure 31: ECG-triggered high-pitch thoraco-abdominal CTA in a patient with an abdominal aortic stent graft using 80 kV X-ray tube voltage. Scan speed 737 mm/s, scan length 592 mm, scan time 0.8 s, heart rate 63 bpm. DLP = 97.5 mGy cm, corresponding to an effective dose of ~ 1.4 mSv. Courtesy of University Hospital Zurich, Switzerland.

Initial publications (Higashigaito et al., 2016; Bittner et al., 2016) have shown the feasibility of contrast agent reduction in long-range aortic scans with high-pitch acquisition. Furthermore, Wielander et al. (2016) has demonstrated that non-triggered high-pitch dual source CTA of the ascending aorta provides excellent image quality.

4. Low-kV scanning of adult and obese patients to reduce radiation dose and/or contrast agent

Siemens Healthineers has pioneered the trend of low-kV scanning with the introduction of 80 kV and 70 kV imaging with the Straton® X-ray tube and the SOMATOM Definition Flash DSCT scanner.

Most CT scans are performed using iodinated contrast agent. It is well documented (e.g., McCollough et al., (2009)) that the X-ray attenuation of iodine, and as a consequence, its CT number in a CT image (in Hounsfield units HU), increases as the mean energy of the X-ray beam decreases, i.e. with the use of lower X-ray tube voltages (kV), see Fig. 32. This behavior is caused by the k-edge of iodine at 33 keV. The X-ray attenuation of soft tissue and fat is influenced only minimally by the X-ray tube voltage. Therefore, the image contrast of tissues and vessels that take up iodinated contrast agent in a contrast-enhanced CT scan improves at lower X-ray tube voltages compared with other surrounding tissues.

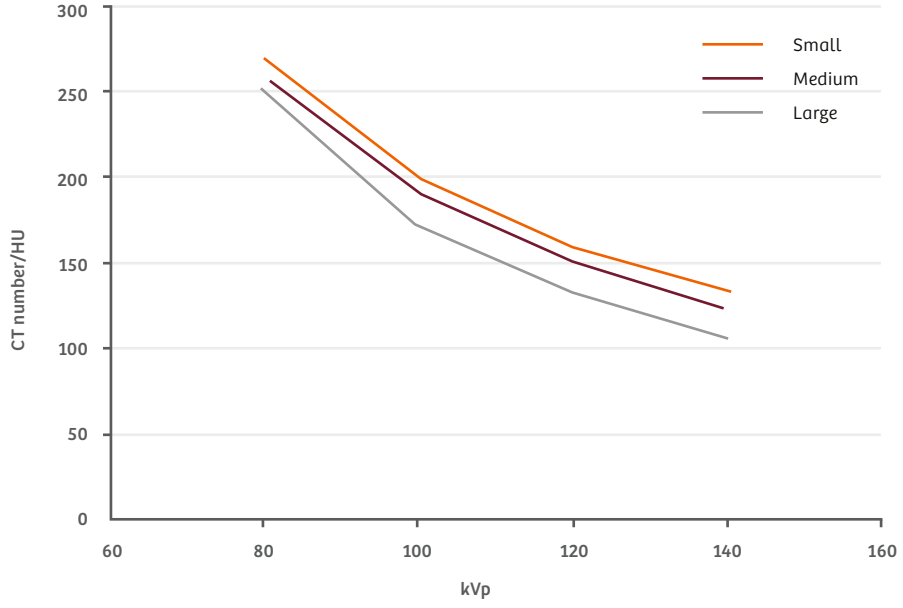

Figure 32: CT number of iodine (in HU) as a function of the X-ray tube voltage for phantoms of different diameters, representing small, medium, and large patients. Note the increase as the X-ray tube voltage kVp decreases. (McCollough et al., 2009).

If the radiation dose applied to the patient during the CT scan is kept constant when using lower X-ray tube voltages (lower kV), the increased contrast of iodine in the image translates into an increased iodine contrast-to-noise ratio (CNR), see Fig. 33.

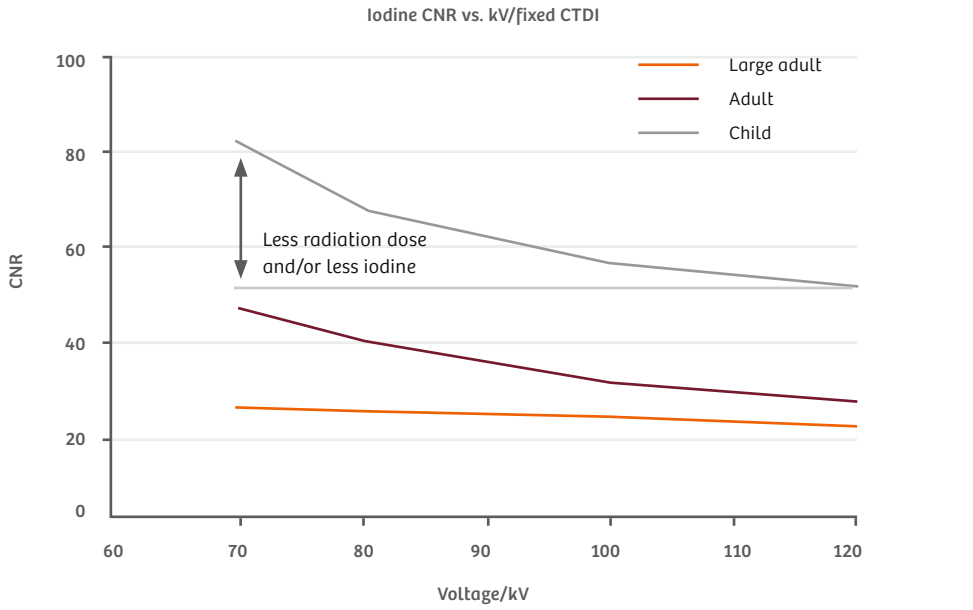

Figure 33: Iodine contrast-to-noise ratio (CNR) with a fixed radiation dose (fixed CTDI) as a function of the X-ray tube voltage (kV) for phantoms representing the attenuation of children, adults, and large adults (internal measurements). A small tube filled with diluted iodine solution was placed at the center of the phantoms; the iodine concentration was chosen to provide the typical contrast of the aorta in a CT angiographic examination. Note the increase in the CNR as the X-ray tube voltage decreases.

If the CNR at the standard X-ray tube voltage of 120 kV used in most CT examinations (referred to as refCNR) is considered adequate for the diagnostic task by the radiologist, the increased CNR at the lower X-ray tube voltage may be exploited to either reduce the radiation dose (and allow for a higher image noise to maintain refCNR), or to reduce the amount of iodinated contrast agent at lower kV. Unfortunately, as the X-ray tube voltage decreases, the image noise at a constant X-ray tube current-time product mAs increases significantly, see for example (Siegel, 2004) and Fig. 34. This is a consequence of the reduced tube output (reduced radiation dose) at a constant tube current mA and at lower kV.

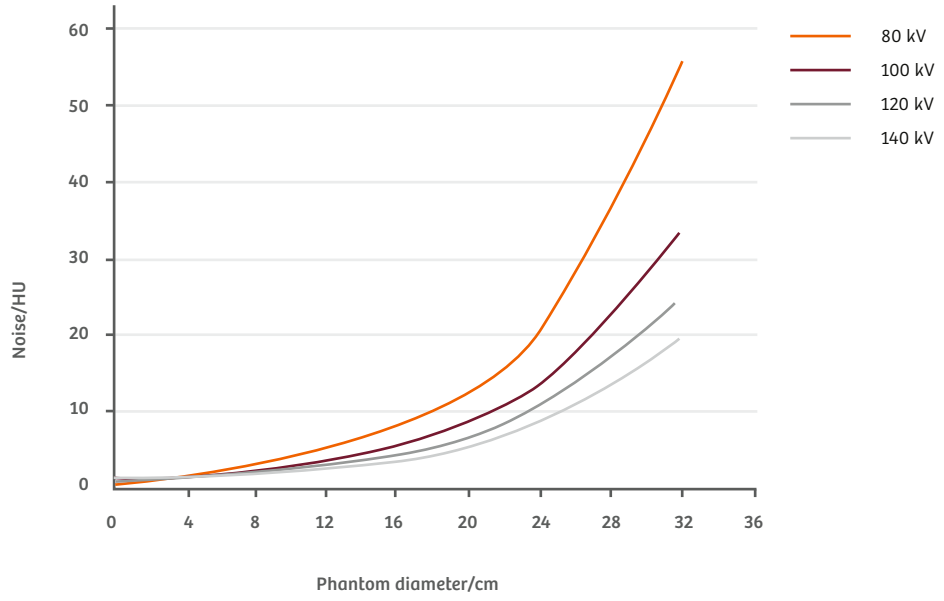

Figure 34: Image noise as a function of the phantom diameter for different X-ray tube voltages at a constant 165 mAs tube current-time product. For a given phantom diameter, image noise at constant mAs increases significantly as the X-ray tube voltage decreases. From (Siegel, 2004).

To maintain the adequate radiation dose (CTDI) when using dual source kV, the tube current-time product mAs has to be significantly increased, in particular for larger patient diameters. If the power reserves of the X-ray tube at low voltages are insufficient to increase the tube current mA to the necessary level, the resulting images will suffer from increased image noise and degraded CNR.

With previous CT scanners, low-kV imaging has been used for children and small patients to reduce the radiation dose and/or the amount of contrast agent, for example in patients with a low BMI < 23 kg/m2 (Cao et al., 2014) or in 181 patients with low body weight (Komatsu et al., 2013). Low-kV imaging could not be adequately applied to adults and larger patients because of insufficient mA reserves of the X-ray tubes at lower kV.

A significant increase in mA reserves and in power at low kV have been implemented in the Vectron™ tube used in SOMATOM Force (see Fig. 3). This facilitates low-kV scanning for adults and larger patients, too, who can benefit from the increased CNR at low kV, and a reduction in the radiation dose and / or the amount of iodinated contrast.

Radiologists at the Clinical Innovation Center, Mayo Clinic Rochester, Minnesota, USA, have demonstrated a radiation dose reduction of 33% and a decrease in the amount of contrast agent of 50% for abdominal imaging using SOMATOM Force at 80 kV, compared with the standard 120 kV using previous CT technology. Figs. 35 and 36 are representative clinical examples. Fig. 37 demonstrates the successful application of low-kV scanning of a morbidly obese patient.

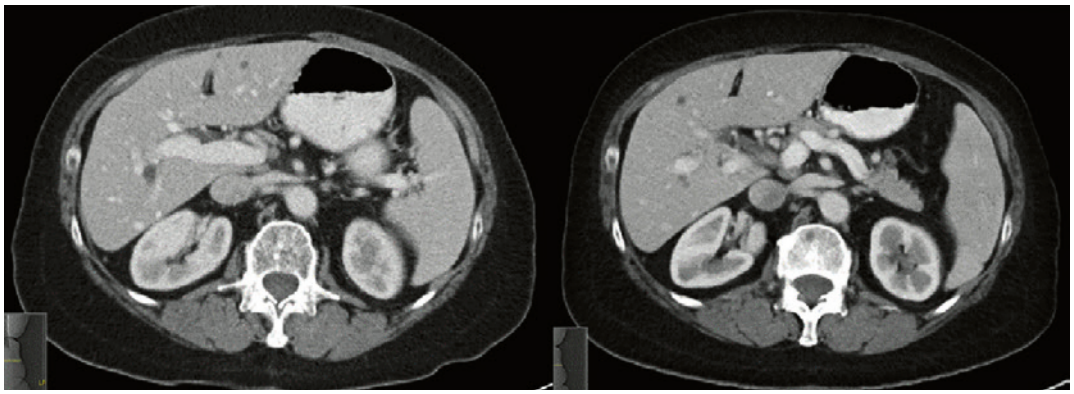

Figure 35: Follow-up examination of a 70-year old male patient. Left: Initial CT scan using previous CT technology in May 2012. 120 kV, 140 mL contrast agent (Omnipaque 300), $CTDI_{vol}$ = 15 mGy. Right: Follow-up CT scan using SOMATOM Force in May 2014. 80 kV, 70 mL contrast agent (Omnipaque 300), $CTDI_{vol}$ = 10 mGy. Despite a reduction in the radiation dose of 33% and a reduction in the amount of contrast agent of 50%, the 80 kV images on SOMATOM Force are of equivalent diagnostic quality. Courtesy of the Clinical Innovation Center, Mayo Clinic Rochester, Minnesota, USA.

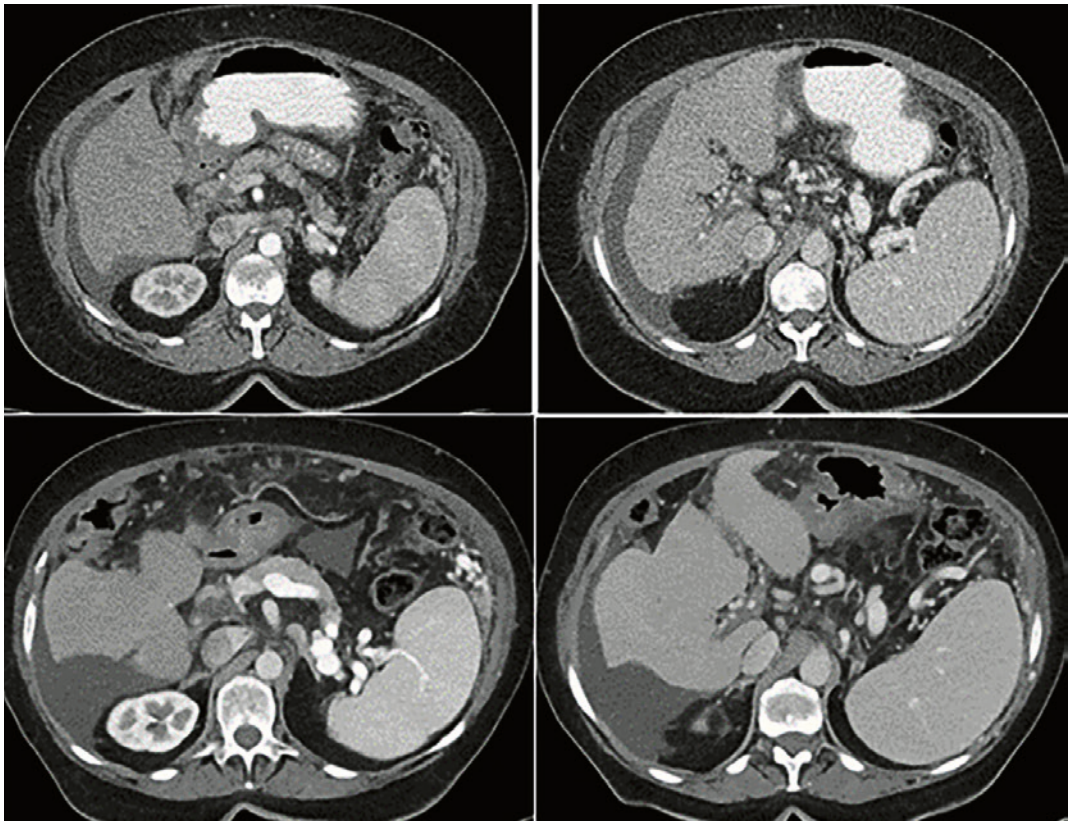

Figure 36: CT scan of a 59-year-old female patient with diabetes, sarcoidosis, and cirrhosis, in order to rule out HCC. Top row: Prior CT exam using previous CT technology in 2008. 120 kV, 140 mL contrast agent, $CTDI_{vol}$ = 18 mGy. Bottom row: CT scan using SOMATOM Force in May 2014. 80 kV, 80 mL contrast agent (Omnipaque 300), $CTDI_{vol}$ = 12 mGy. Despite a reduction in the radiation dose of 33% and a reduction in the amount of contrast agent of 43%, the 80 kV images on SOMATOM Force show superior image quality. Courtesy of the Clinical Innovation Center, Mayo Clinic Rochester, Minnesota, USA.

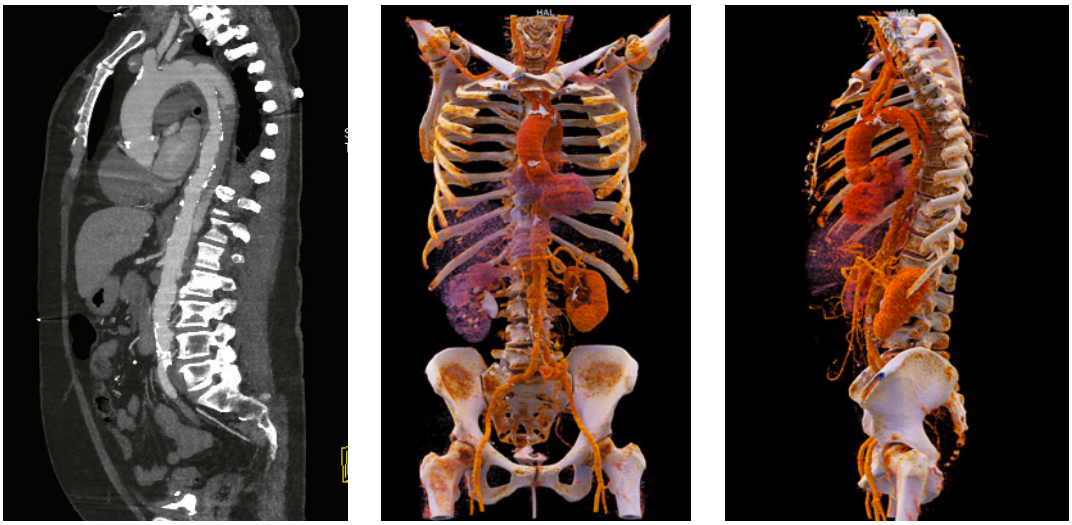

Figure 38: Whole body CT angiographic examination in a patient with impaired less perfused right kidney with Stanford type B dissection of the aorta on SOMATOM Force. Turbo Flash high-pitch spiral with scan speed 737 mm/s, 80 kV tube voltage, 20 mL iodinated contrast agent. DLP = 154.6 mGy cm, corresponding to an effective dose of ~ 2.2 mSv. Courtesy of Institute of the Diagnostic Radiology, Mannheim University, Germany.

Meyer (Meyer et al. , 2014) prospectively evaluated the radiation dose and contrast medium requirements for performing high-pitch coronary CTA at 70 kV using SOMATOM Force compared with a previous generation CT scanner. Forty-five patients (median age 52 years; 27 men) were imaged in high-pitch mode using SOMATOM Force at 70 kV (n = 15, BMI ≤ 26 kg/m²) or with the previous DSCT system at 80 kV (n= 15, BMI ≤ 26 kg/m²) or 100 kV (n = 15, 26 kg/m² < BMI ≤ 30 kg/m²). Qualitative image quality analyses revealed no significant differences between the three CTA protocols. The mean effective dose was 0.92 mSv for the 100 kV protocol, 0.78 mSv for the 80 kV protocol, and 0.44 mSv for the 70 kV protocol. The authors conclude that "in non-obese patients, third-generation high-pitch coronary DSCT angiography at 70 kV results in robust image quality for studying the coronary arteries, at significantly reduced radiation dose (0.44 mSv) and contrast medium volume (45 mL), thus enabling substantial radiation dose and contrast medium savings". The authors further state that "this may be particularly important in young patients and those with renal insufficiency. "The extent to which the 70 kV coronary CTA protocol can be adapted to obese patients with a BMI of more than 26 kg/m² has to be evaluated in future studies. Fig. 39 shows a clinical example (Meyer et al., 2014).

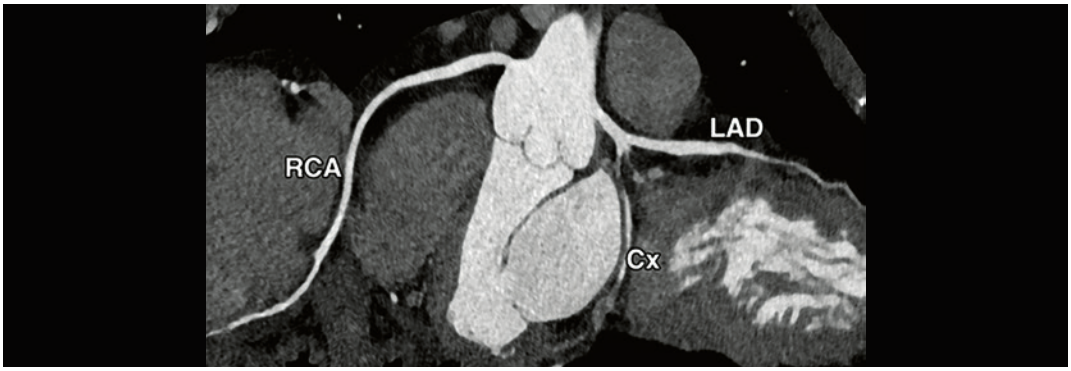

Figure 39: Coronary CTA in a 45-year-old man with chest pain and a heart rate of 64 bpm. Turbo Flash high-pitch spiral at 70 kV with an effective dose of 0.21 mSv. Curved multiplanar reformation (MPR) along the right coronary artery (RCA) and the left anterior descending (LAD) coronary artery (Meyer et al., 2014).

Meinel et al. (Meinel, 2014) assessed the influence of the X-ray tube voltage on the radiation dose and image quality of third-generation DSCT coronary angiography in a phantom simulating an obese patient. The authors conclude that third-generation DSCT offers substantially increased tube power at low tube potential. This enables one to perform coronary CT angiography at 70–80 kV in obese patients. Signal-to-noise ratio is maintained owing to increased tube current. This approach can be expected to reduce radiation dose by 49–68%". Fig. 40, combining two figures from (Meinel et al., 2014), shows CNR as a function of the tube potential for the third-generation DSCT system SOMATOM Force and the corresponding volume CT dose index ($CTDI_{vol}$). The percentage numbers indicate the potential radiation dose reduction at 70–100 kV compared with a 120 kV acquisition on the same CT system.

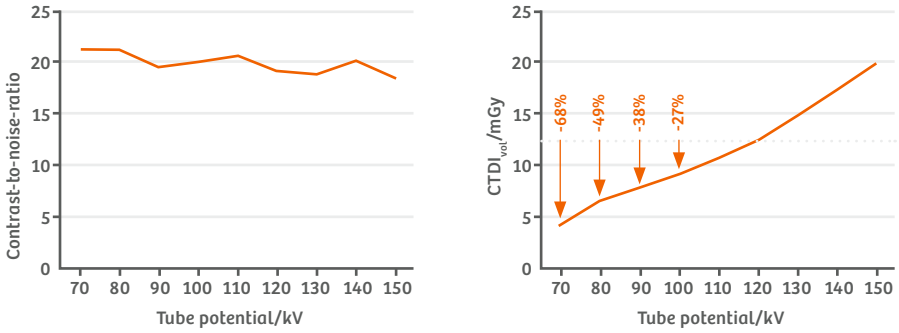

Figure 34: Image noise as a function of the phantom diameter for different X-ray tube voltages at a constant 165 mAs tube current-time product. For a given phantom diameter, image noise at constant mAs increases significantly as the X-ray tube voltage decreases. From (Siegel, 2004).

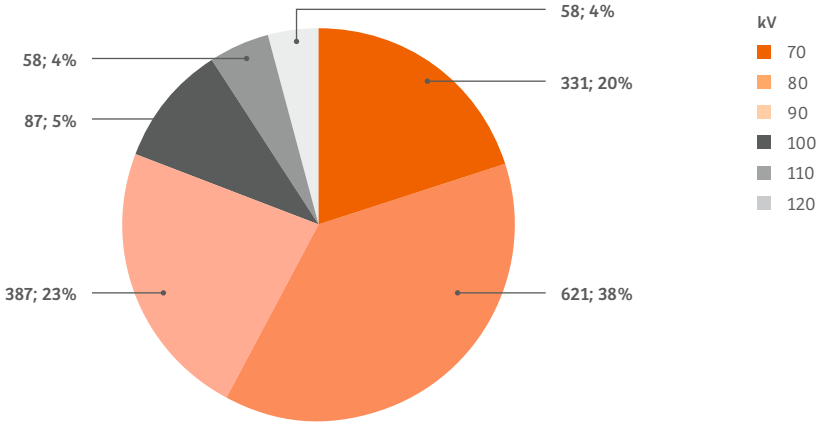

Figure 41: Evaluation of a German SOMATOM Force site with 1,650 cardiac patients in clinical routine within one and a half years. 81% were scanned with kV settings below 100 kV and none above 120 kV. This shows the capability of low-kV imaging in clinical routine with SOMATOM Force.

5. Spectral prefiltration in combination with ADMIRE to significantly reduce radiation dose in non-enhanced CT scans

A very low radiation dose is especially important in CT examinations of lungs and the colon for early disease detection, to search for kidney stones or to diagnose sinusitis.

For these examinations, which are typically performed without iodinated contrast agent, SOMATOM Force has two Tin (Sn) Filters, one for each X-ray tube. These Tin Filters can be moved into the X-ray beam in the pre-patient tube collimator boxes if needed.

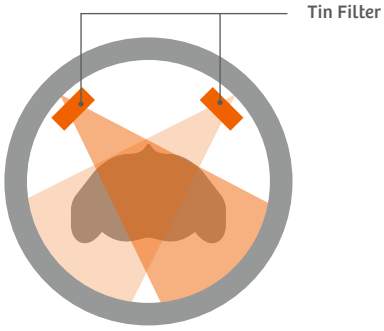

Figure 42: SOMATOM Force has two Tin Filters inside the X-ray sources. These can be utilized in different scan modes for a spectral prefiltration to remove the lower-energy X-ray photons. This CT technology is unique to Siemens Healthineers.

They remove the lower-energy X-ray photons from the X-ray spectrum and harden it, i.e. they shift the mean energy to higher values. Figure 43 (Gordic et al., 2014)demonstrates the effect of tin prefiltration on the shape of the spectra for 100 kV + Tin Filter (100 Sn kV) and 150 kV + Tin Filter (150 Sn kV). Note the onset of the tin-filtered spectra at around 50 keV as compared to about 30 keV for the standard 70 kV and 120 kV spectra.

Removing the lower-energy X-ray quanta from the X-ray spectrum and hardening it is beneficial in CT examinations that do not use iodinated contrast agent. When using standard CT technology without spectral prefiltration, these lower-energy X-ray quanta are absorbed in the patient without contributing to the measured signal. They degrade the dose efficiency of non-enhanced CT scans, which then require a higher radiation dose[2]. Furthermore, beam-hardening artifacts are significantly reduced using spectral prefiltration.

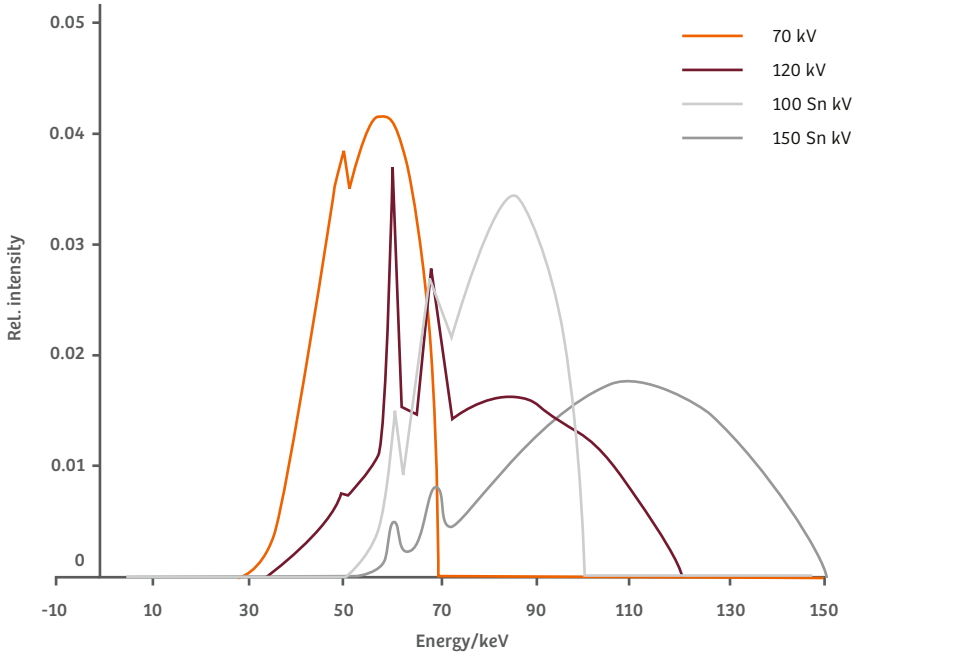

Figure 43: Spectral shaping by tin prefiltration. The standard 70 kV and 120 kV spectra are compared to 100 kV and 150 kV spectra with tin prefiltration (100 Sn kV, 150 Sn kV). Note the removal of lower-energy quanta (in the range of 30 keV to 50 keV) from the tin-filtered spectra (Gordic et al., 2014).

Fig. 43 demonstrates the dose reduction potential for non-enhanced CT scans (as in lung and colon imaging, or for the detection of kidney stones) when using Tin Filters to shape the X-ray spectrum.

[2] When iodine is used, the increasing iodine contrast at low kV more than compensates for the reduced dose efficiency at low kV. Contrast-enhanced CT examinations should therefore be performed at low X-ray tube voltages to reduce radiation dose, see section 4. The iodine K-edge at 33 keV is also the reason why standard CT systems without moveable prefilters do not use stronger prefiltration to harden the spectra – then, iodine contrast would be lost.

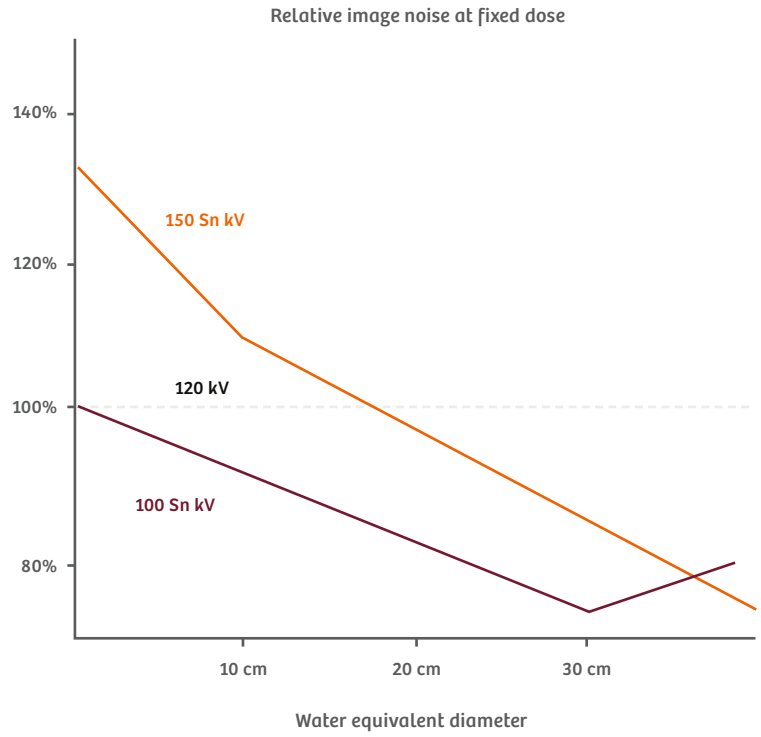

Figure 44: Relative image noise (normalized to the image noise at 120 kV) as a function of the water equivalent diameter of various phantoms, for the same radiation dose but different X-ray spectra: 120 kV, 100 kV + Tin Filter (100 Sn kV), 150 kV + Tin Filter (150 Sn kV). Results from Siemens Healthineers in-house measurements.

Note that at 100 Sn kV (100 kV X-ray tube voltage + tin prefiltration), the image noise at a constant radiation dose is always lower than at the standard X-ray tube voltage of 120 kV (for all water equivalent diameters). In the X-ray attenuation range of lung and colon examinations, corresponding to 20–35 cm water equivalent diameter, the image noise is up to 30% lower compared with the standard 120 kV setting. This can be translated into a potential radiation dose reduction of up to 50% when using 100 Sn kV[3].

Gordic et al. (Gordic, 2014) evaluated the image quality and sensitivity of ultra-low radiation dose single energy CT with tin (Sn) filtration for spectral shaping, and the iterative reconstruction for the detection of pulmonary nodules in a phantom setting using SOMATOM Force in comparison with a previous generation scanner. Figure 45 shows the experimental setup. Two patients were included for proof of concept.

With SOMATOM Force, the phantom scans were performed at 70 kV, 100 Sn kV, and 150 Sn kV, the authors' standard dose of a thorax examination ($CTDI_{vol}$ = 3.1 mGy), 1/10th of the standard dose (0.31 mGy), and 1/20th of the standard dose (0.15 mGy). With the previous scanner generation, the phantom scans were performed at 120 kV the lowest possible radiation dose at that tube voltage (0.28 mGy).

[3] Since the image noise depends on the square root of the radiation dose, image noise reduction of 30% to 0.7 of the original value can be "compensated" by a radiation dose reduction to 0.7•0.7 = 0.49 of the original dose value, i.e. of 50%.

With the previous scanner, the image noise at 120 kV and 0.28 mGy ranged from between 256 and 277 HU using SAFIRE Level 3 iterative reconstruction. With SOMATOM Force, the image noise at 100 Sn kV and 1/20th of the standard dose (0.15 mGy) ranged from between 214 and 229 HU using ADMIRE Level 3 iterative reconstruction, and between 105 and 111 HU using ADMIRE Level 5, see Fig. 46. SOMATOM Force provided lower image noise at 100 Sn kV and 0.15 mGy than the previous CT system at the commonly used standard X-ray tube voltage of 120 kV and almost twice the radiation dose (0.28 mGy versus 0.15 mGy).

Gordic et al. further concluded that the sensitivity of pulmonary nodule detection was lowest and the number of false-positives was highest in images acquired using the previous scanner generation at 120 kV and 0.28 mGy. Sensitivity was higher, and the number of false-positives was lower, with the third-generation DSCT at 100 Sn kV, both at 0.31 mGy and at 0.15 mGy.

According to Gordic et al., the patient images acquired with SOMATOM Force using 100 Sn kV were of diagnostic quality both at 1/10th of the standard dose (corresponding to an effective patient dose of about 0.13 mSv) and at 1/20th of the standard dose (corresponding to an effective patient dose of about 0.07 mSv).

The authors conclude that "chest CT for the detection of pulmonary nodules can be performed with third-generation DSCT producing high image quality, sensitivity, and diagnostic confidence at a very low effective radiation dose of 0.06 mSv when using a single-energy protocol at 100 kVp with spectral shaping and when using advanced iterative reconstruction techniques". Note that this is the dose level of a chest X-ray examination.

Figs. 47 and 48 show representative clinical cases demonstrating ultra-low dose lung imaging with SOMATOM Force.

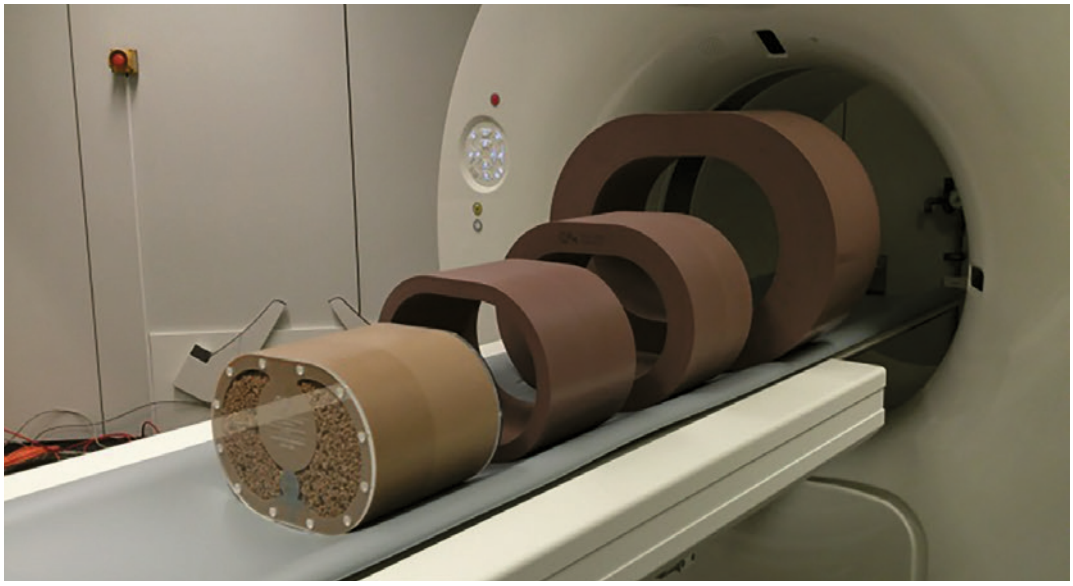

Figure 45: Anthropomorphic thorax phantom used for the evaluation of ultra-low dose chest CT for pulmonary nodule detection. The phantom (left) has a lateral diameter of 35 cm and an anteroposterior diameter of 25 cm. The first extension ring of 2.5 cm thickness was used to simulate realistic attenuation. The phantom contains 18 solid pulmonary nodules of various sizes (2–10 mm; attenuation 75 HU at 120 kV). Each of these nodules is surrounded by cork granulate material with an air equivalent CT number. See also (Gordic et al., 2014).

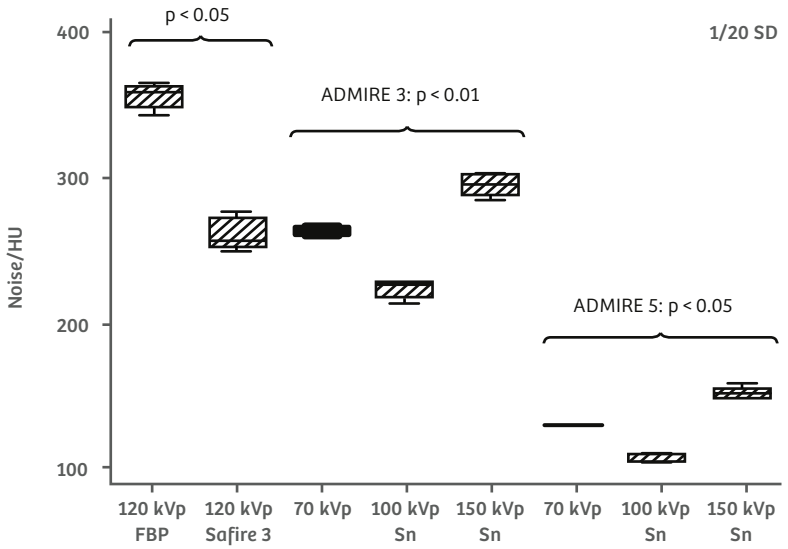

Figure 46: Image noise for the standard 120 kV spectrum with filtered back projection (FBP) and SAFIRE 3 at 0.28 mGy, and for 70 kV, 100 Sn kV, and 150 Sn kV with ADMIRE 3 and ADMIRE 5 at 0.15 mGy (1/20 SD). The protocol with 100 Sn kV was associated with the lowest image noise (Gordic et al., 2014).

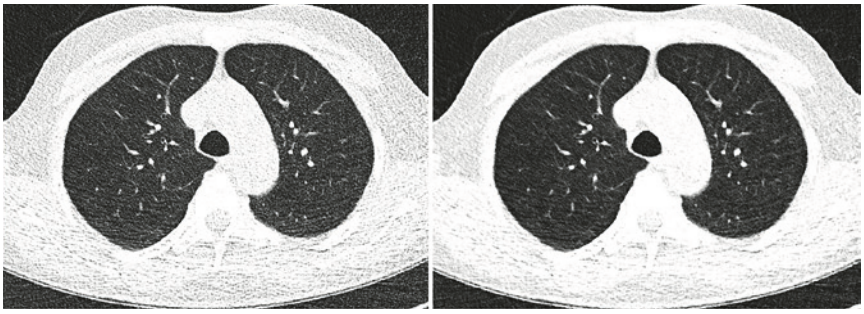

Figure 47: Representative transverse CT sections of a patient scanned at 1/10th dose (effective dose ~ 0.13 mSv) with 100 Sn kV. Images were reconstructed with ADMIRE 3 (left) and ADMIRE 5 (right). (Gordic et al., 2014).

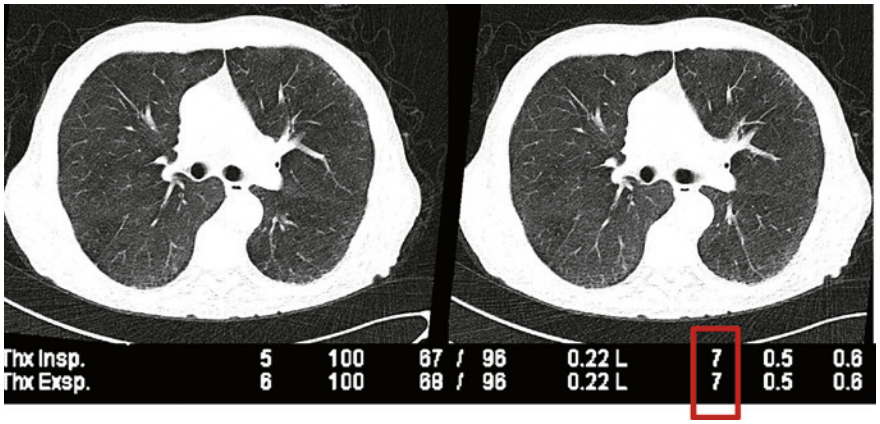

Figure 48: Non-enhanced CT scan of the lung in a patient with atypical pneumonia in inspiration and expiration, using 100 Sn kV in combination with the Turbo Flash high-pitch spiral mode and ADMIRE iterative reconstruction. DLP = 7 mGy cm, corresponding to an effective dose of ~0.1 mSv per scan.
Courtesy of the Institute of Diagnostic Radiology, Mannheim University, Germany.

6. Improved performance and spectral separation of Dual Energy CT: from morphology to functional evaluation

Within recent years, Dual Energy CT has found its way into clinical routine (see Barrett et al. (2011), Schenzle et al. (2010), Sudarski et al. (2015), Uhrig et al. (2016). Wortman et al. (2016) have published an overview of different clinical applications in the abdomen and the reduced need for follow-up imaging.

The quality of Dual Energy CT examinations relies on the effective separation of the energy spectra Krauss et al., (2015). Spectral overlap and poor energy separation mean less efficient and less precise tissue differentiation, which must then be compensated by increasing the radiation dose.

SOMATOM Force utilizes multiple combinations of different X-ray spectra for the acquisition of DE data. Compared to previous CT technology, energy separation has been improved by:

- Providing 150 kV X-ray tube voltage with more aggressive tin prefiltration (0.6 mm) to acquire the high-energy CT data, instead of 140 kV with no or less aggressive tin prefiltration (0.4 mm) with previous CT technology.
- Providing 70 kV, 80 kV, 90 kV X-ray tube voltages with significantly increased tube current of the Vectron X-ray tube at low-kV to acquire the low-energy CT data, with sufficient power reserves to scan adults and larger patients (see also section 1).

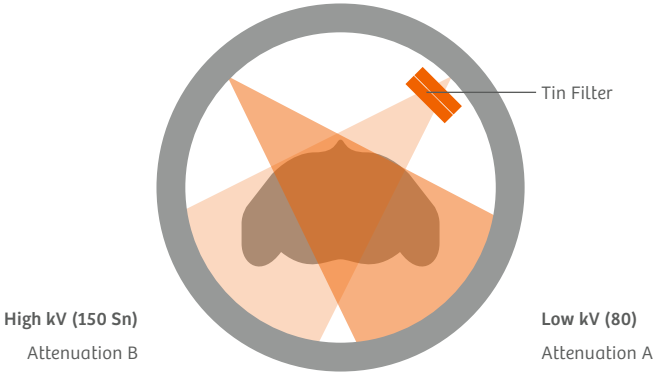

Figure 49: The principle of a Dual Energy scan. While attenuation A uses a low kV (i.e. 80 kV) setting, attenuation B uses a tin-filtered high kV setting (i.e. 150 kV). This offers excellent spectral separation.

One way of quantifying the performance of a Dual Energy CT acquisition technique with regard to energy separation and the material differentiation capability is the use of dual energy ratios. The DE ratio of a material is defined as its CT number (in HU) at low kV divided by its CT number at high kV. As a representative example, we focus on the DE ratio of iodine.

A frequently used Dual Energy application relies on the acquisition of Dual Energy CT data when an iodinated contrast agent is used (e.g., to examine the liver). The spectral information is then used to compute both an iodine image, which visualizes the iodine uptake in different tissues, and a virtual non-enhanced image with the iodine removed, which corresponds to a true non-enhanced CT image without the administration of contrast agent, see e.g., (Zhang et al., 2010). The DE iodine ratio is generally independent of mAs and other reconstruction parameters. Using the thin absorber model, the DE iodine ratio depends only very slightly on the iodine concentration. Under the assumption that image noise in the low- and high-kV image is the same, the image noise in virtual non-enhanced images only depends on the DE iodine ratio and decreases as the DE iodine ratio increases. The higher the DE iodine ratio, the better the quality of the virtual non-enhanced images, and the greater the precision with which the iodine can be differentiated and quantified.

We measured DE iodine ratios and image noise in virtual non-enhanced images for different Dual Energy CT acquisition techniques and in different CT scanner generations in a phantom study (Krauss et al., 2015). Using circular phantoms made of water equivalent material of different diameters (10, 20, 30, and 40 cm), representing patients of different sizes, with a small tube (diameter 2.0 cm) inserted at the center which was filled with diluted contrast agent (15 mg/mL Ultravist solution, representing the typical attenuation of an aorta with contrast agent). The CT value was measured of iodine within a centered region of interest (ROI) with a diameter of 1 cm. Fig. 50 shows the measured DE iodine ratios at a phantom diameter of 20 cm for previous CT scanners (kV switching, DSCT SOMATOM Definition, DSCT SOMATOM Definition Flash) and for SOMATOM Force.

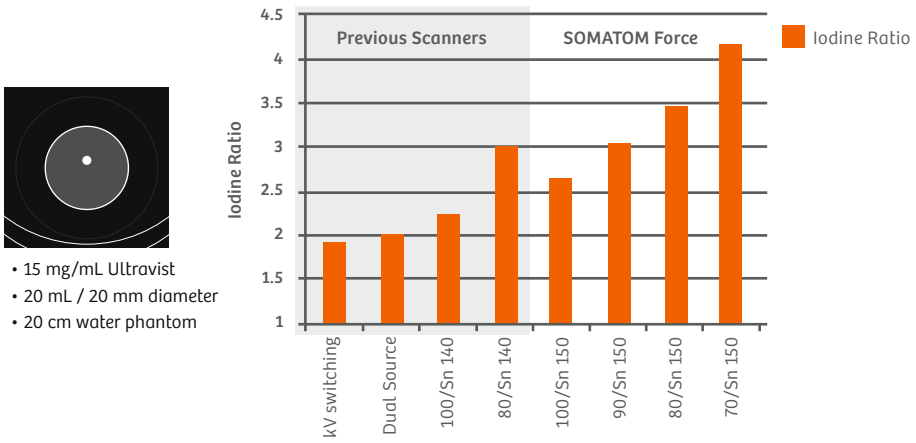

Figure 50: DE iodine ratios for different DE acquisition techniques at 20 cm phantom diameter: kV switching 80 kV / 140 kV, Dual Source at 80 kV / 140 kV, at 100 kV / kV and at 80 kV / 140 Sn kV (0.4 mm tin pre-filtration), SOMATOM Force at 100 kV / 150 Sn kV, at 90 kV / 150 Sn kV, at 80 kV / 150 Sn kV and at 70 kV / 150 Sn kV (in this case, Sn indicates the use of tin prefiltration). Note the significant increase in DE iodine ratios with SOMATOM Force as compared with previous technologies.

The DE iodine ratio for SOMATOM Definition Flash at the standard X-ray tube voltage combination 100 kV / 140 Sn kV is 2.25; the DE iodine ratio for SOMATOM Force at the new standard X-ray tube voltage combination 90 kV / 150 Sn kV is 3.0. This corresponds to an improvement of 33%. When comparing the best available scan options (with regard to DE iodine ratio) of SOMATOM Definition Flash (80 kV / 140 Sn kV with a DE iodine ratio of 3.0) and SOMATOM Force (70 kV / 150 Sn kVwith a DE iodine ratio of 4.15), the improvement using SOMATOM Force is 38%. When comparing the standard 90 kV / 150 Sn kV scan mode of SOMATOM Force with scan techniques relying on the use of 80 kV / 140 kV without spectral shaping (such as kV switching), the improvement using SOMATOM Force is 58%.

The DE ratio for other phantom diameters is shown in Fig. 51 (Krauss et al., 2015).

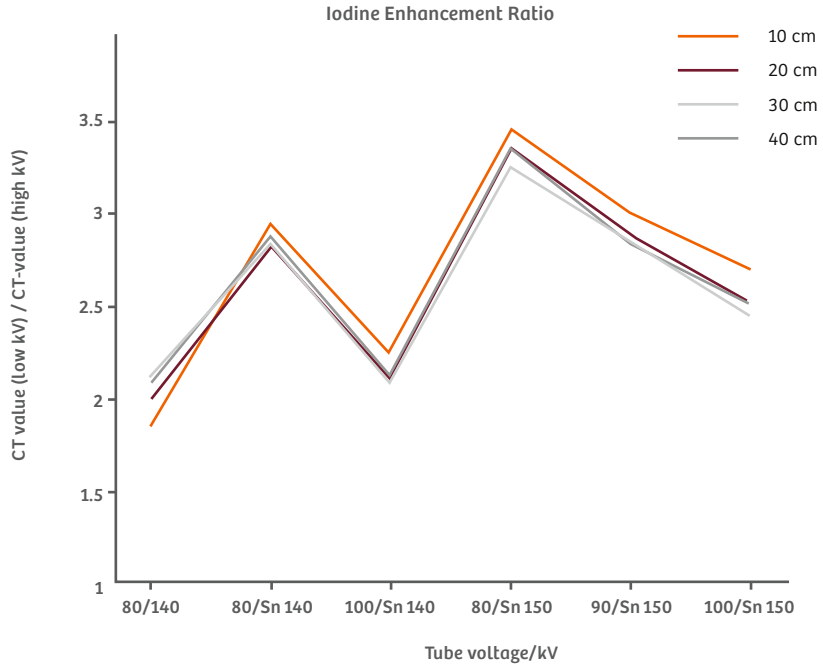

Figure 51: DE iodine ratios for different DE acquisition techniques at different phantom diameters.

Fig. 52 shows the measured image noise in virtual non-contrast (VNC) images at the same radiation dose. The $CTDI_{vol}$ values for the 10, 20, 30, and 40 cm phantoms (1.2, 2.5, 7.2, and 21.2 mGy) were applied to all voltage combinations used to scan the respective phantoms. Image noise in VNC images is a good indicator for the radiation dose efficiency of a DE technique: the lower the image noise in the VNC images after DE material decomposition, the less radiation dose has to be used for DE scanning in order to obtain VNC images that can replace true non-contrast images. At the same radiation dose, the noise is highest at 80 / 140 kV, and lowest at SOMATOM Force settings using 150 Sn kV. For all phantom sizes, the noise in the VNC images is lowest for the 80 kV / 150 Sn kV combination. For the 40 cm phantom, the image noise at 80 kV / 140 kV without spectral shaping is 117% higher than at 80 kV / 150 Sn kV.

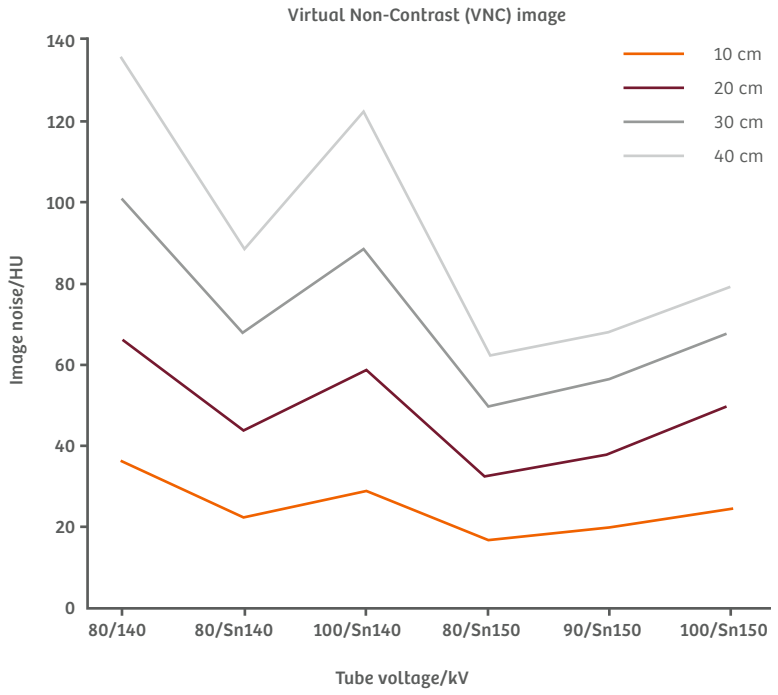

Figure 52: Image noise in the VNC images for different DE acquisition techniques at different phantom diameters. At each phantom diameter, the radiation dose was kept constant for the different techniques. The lower the image noise in a VNC image, the better the radiation dose efficiency of the respective DE technique.

Researchers at the Clinical Innovation Center, Mayo Clinic Rochester, Minnesota, USA, have used SOMATOM Force to demonstrate how to achieve a more precise differentiation of similar tissues using Dual Energy scanning than with previous technologies, thanks to the improved energy separation of SOMATOM Force.

They performed a phantom study and scanned 88 human urinary stone samples that were immersed in plastic vials of saline in a water-filled 35 cm water tank with an anthropomorphic shape, see Fig. 53.

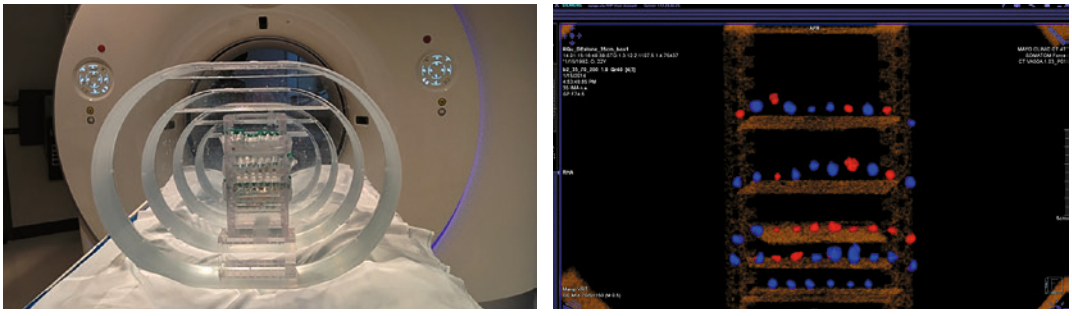

Figure 53: Left: Experimental setup to scan human urinary stone samples immersed in plastic vials of saline in a water-filled 35 cm water tank and with an anthropomorphic shape. Right: DE image with color-coded kidney stones. Uric acid stones are highlighted in red; other stones are highlighted in blue. Courtesy of the Clinical Innovation Center, Mayo Clinic Rochester, Minnesota, USA.

The authors measured the DE ratios of different types of kidney stones (uric acid, cystine, calcium oxalate, and apatite) using different DE techniques: the previous voltage combinations 80 kV / 140 Sn kV and 100 kV / 140 Sn kV with tin prefiltration and the new voltage combinations 70 kV / 150 Sn kV, 80 kV / 150 Sn kV, 90 kV / 150 Sn kV and 100 kV / 150 Sn kV with tin prefiltration available on SOMATOM Force. The results are shown in Fig. 54. The authors observed increased DE ratios with 100% accuracy in stone differentiation using SOMATOM Force, with lower image noise at matched radiation dose than in previous CT scanners.

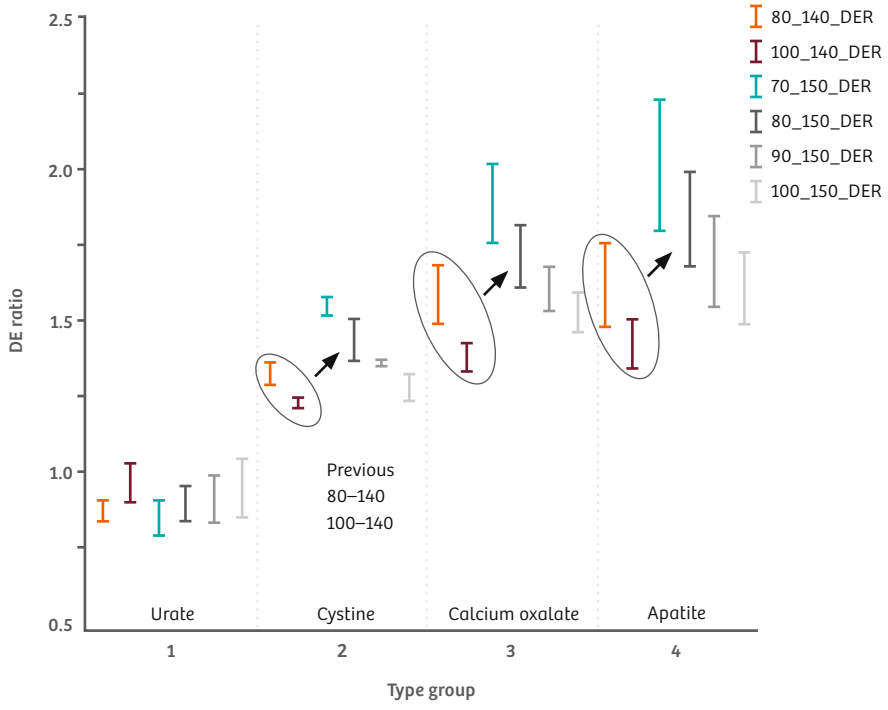

Figure 54: DE ratios for different types of kidney stones using different DE techniques: the previous 80 kV / 140 Sn kV and 100 kV / 140 Sn kV with tin prefiltration and 70 kV / 150 Sn kV, 80 kV / 150 Sn kV, 90 kV / 150 Sn kV and 100 kV / 150 Sn kV with tin prefiltration available on SOMATOM Force. Note the significantly increased DE ratios on SOMATOM Force. Courtesy of the Clinical Innovation Center, Mayo Clinic Rochester, Minnesota, USA.

In addition to the significantly improved energy separation, SOMATOM Force offers a wider scan field of view of 355 mm for DE scanning, and a faster scan speed of up to 258 mm/s, which means that the DE techniques may be adopted in routine clinical practice.

Figure 55 demonstrates kidney stone analysis in a heavy patient (105 kg) using 90 kV / 150 Sn kV. The clinical case shown in Fig. 56 demonstrates a precise DE bone removal in a CT angiographic scan of the head and the neck, while preserving the lumen of the contrast-enhanced vessels and calcified lesions which are also in the vicinity of complex bony structures.

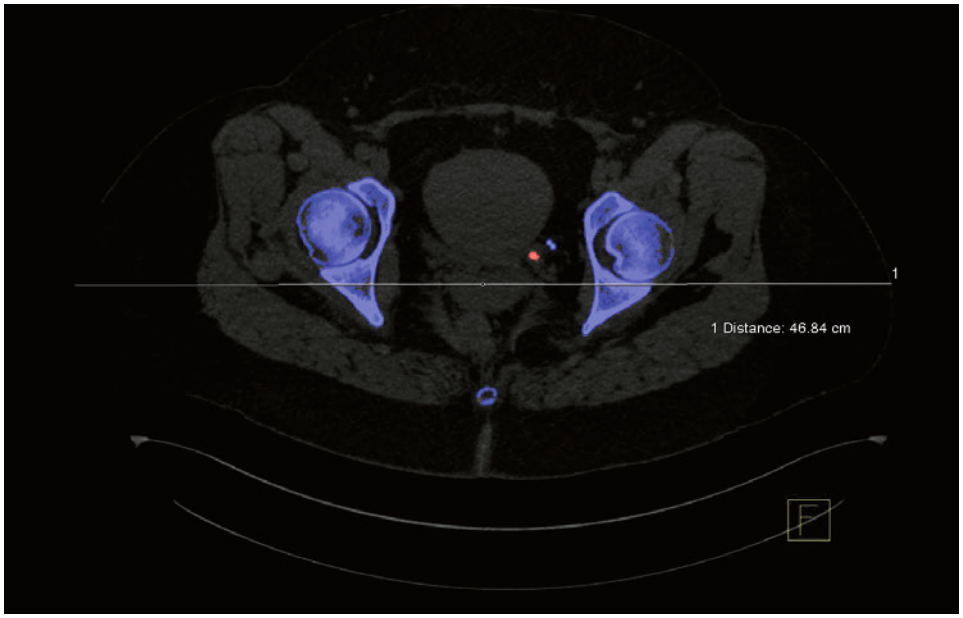

Figure 55: DE kidney stone analysis (red: uric acid) in a heavy patient (105 kg), scanned on SOMATOM Force with 90 kV / 150 Sn kV. Courtesy of the Institute of Diagnostic Radiology, Mannheim University, Germany.

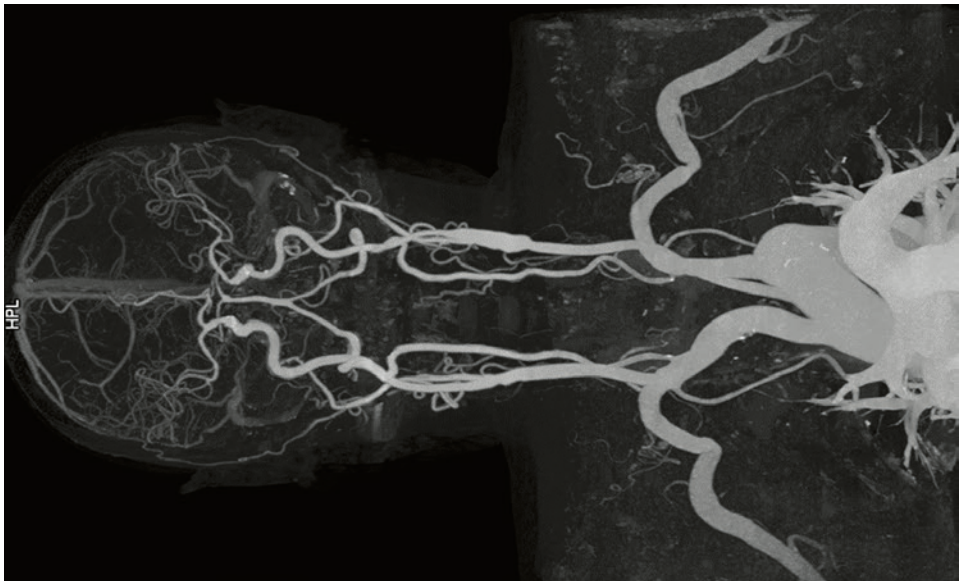

Figure 56: DE bone removal in a CT angiographic scan of the head and neck on SOMATOM Force with 90 kV / 150 Sn kV. Courtesy of the Institute of the Diagnostic Radiology, Mannheim University, Germany.

Fig. 57 demonstrates the visualization of the iodine level in the lung parenchyma as a surrogate marker for the perfused blood volume in a patient who is suspected to have pulmonary embolism, using the new 90 kV / 150 Sn kV DE data acquisition technique on SOMATOM Force. The dark areas in the lung parenchyma demonstrate a reduced iodine content (reduced local perfusion), potentially caused by clots in the pulmonary arteries.

The iodine concentration in the arteries is also indicated: light blue corresponds to higher Iodine concentrations; red corresponds to reduced iodine concentration in the blood vessel.

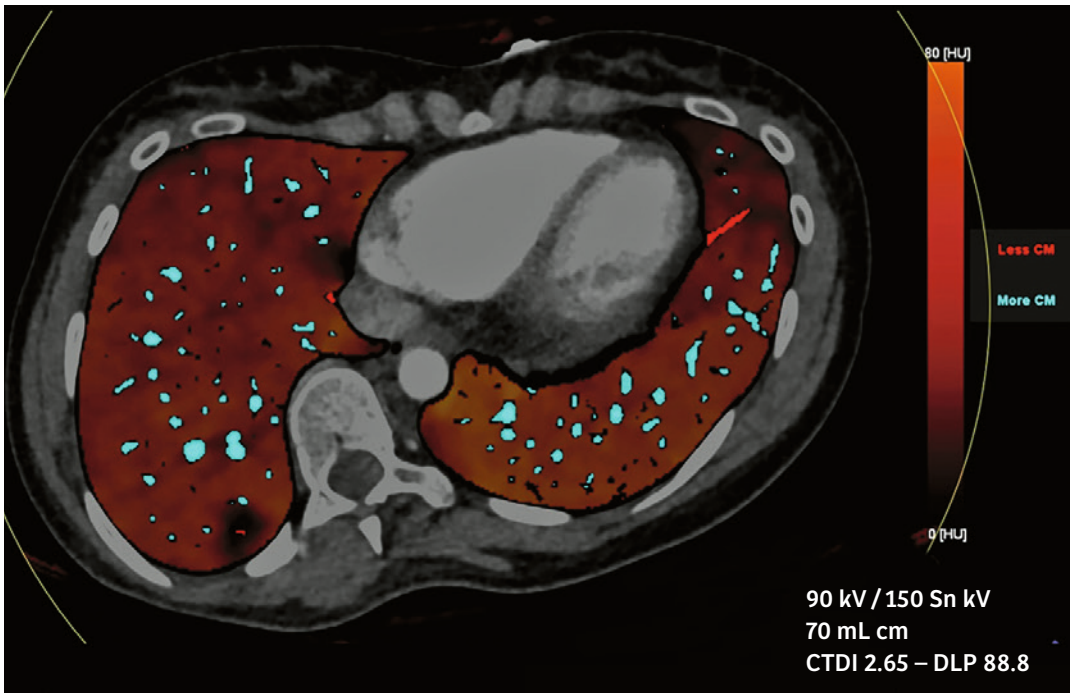

Figure 57: Visualization of the iodine level in the lung parenchyma, and in the lung vessels of a patient suspected to have pulmonary embolism, using the new 90 kV / 150 Sn kV DE data acquisition technique on SOMATOM Force. DLP = 88.8 mGy cm, corresponding to an effective radiation dose of ~ 1.3 mSv.
Courtesy of Klinikum Großhadern, Munich, Germany.

Fig. 58 demonstrates DE decomposition into a virtual non-contrast (VNC) image and an iodine image. Note the good image quality and low image noise of the VNC image as a consequence of the improved energy separation with SOMATOM Force (see also Fig. 52).

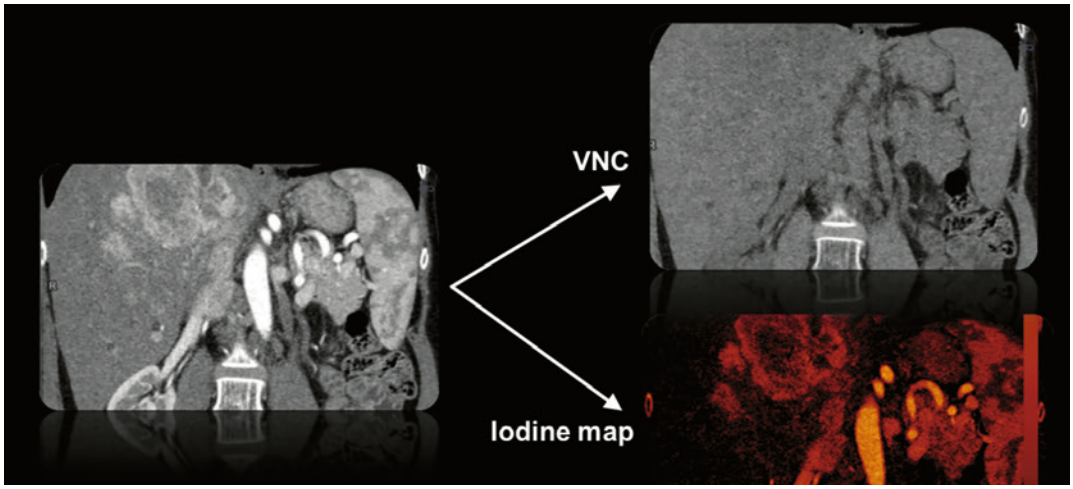

Figure 58: Computation of a virtual non-contrast image and an iodine image from a DE scan at 100 kV / 150 Sn kV.
Courtesy of University Hospital Zurich, Switzerland.

A new algorithm for computing virtual monoenergetic images (energy range 40 keV to 190 keV in intervals of 1 keV) from DE scans is available on SOMATOM Force (Monoenergetic Plus, see (Grant et al., 2014)). To avoid noise increase at lower calculated energies – a known drawback of virtual monoenergetic images at low-keV images with high contrast and high noise (e.g., 40 keV) are non-linearly mixed with images at lower contrast and lower noise (70 keV) to achieve an improved CNR at low-keVs (e.g., 40 keV). The local contribution of both images to the final image depends on the spatial frequency. Monoenergetic Plus can significantly increase the iodine CNR in CT images, and the algorithm can potentially be very useful in improving both detection and differential diagnosis of abdominal lesions (specifically low-contrast lesions). It is also applicable in other anatomical regions where improved iodine CNR is beneficial (Grant et al., 2014).
Fig. 59 is a clinical example illustrating the performance of Monoenergetic Plus.

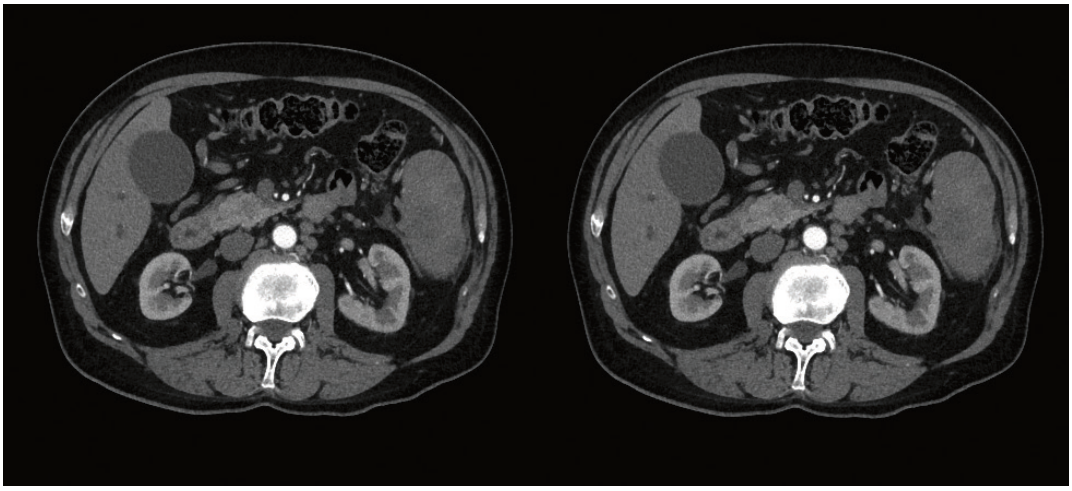

Figure 59: Frellesen et al. (2015) have shown that Dual Energy CT with SOMATOM Force can significantly improve image quality and pancreas-to-lesion contrast in the diagnosis of pancreatic adenocarinoma. In this case, 45 keV Monoenergtic Plus shows better contrast than a mixed image that corresponds to conventional 120 kV image. Courtesy of Northwestern Memorial Hospital, Chicago, USA.

Thanks to the improved spectral separation on SOMATOM Force, ECG-triggered DE images of the heart can be acquired with a very good image quality and a low radiation dose. One relevant clinical application is the computation of iodine images and virtual non-enhanced images from a first-pass coronary CTA in order to visualize and potentially quantify perfusion defects in the myocardium, see e.g., (Vliegenthart et al., 2012). Fig. 60 shows a clinical example acquired on SOMATOM Force. Note the homogeneous iodine distribution in the myocardium without beam hardening or other artifacts in this patient, who does not have myocardial perfusion defects. ECG-triggered DE cardiac CT with the computation of virtual monoenergetic images may also be useful for reducing the artifacts caused by metal implants such as artificial valves, see Fig. 61.

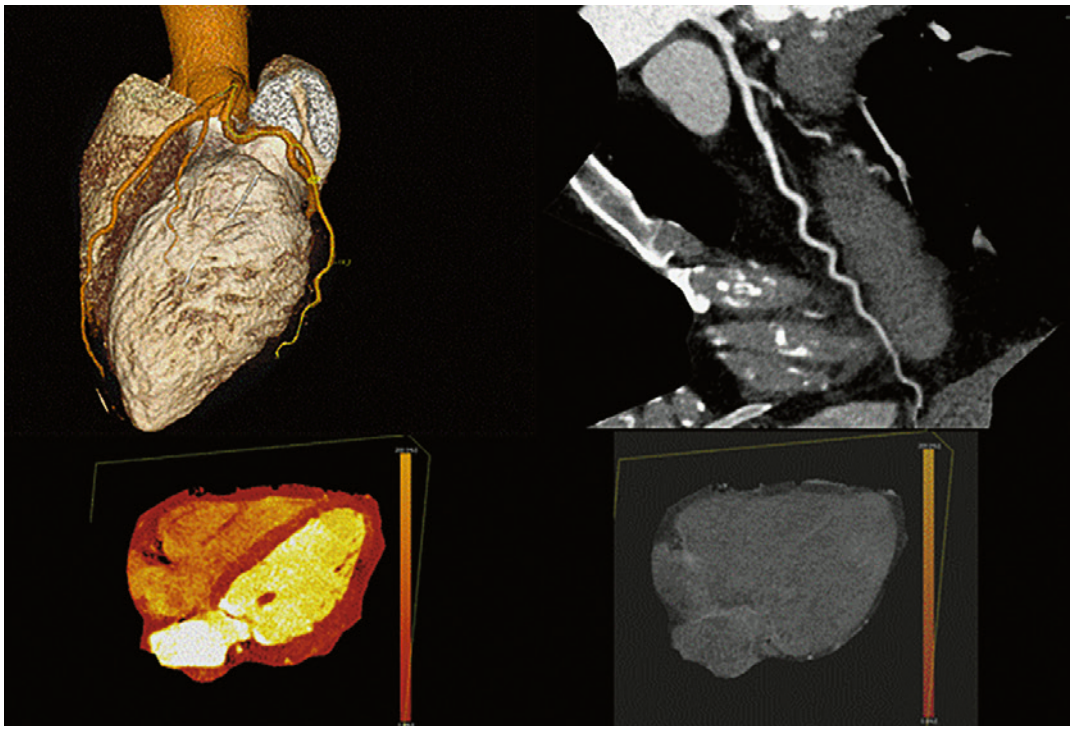

Figure 60: ECG-triggered “step-and-shoot” Dual Energy cardiac CT acquisition. 90 kV / 150 Sn kV, DLP = 145.3 mGy cm, corresponding to an effective radiation dose of ~ 2.2 mSv. Top row: VRT and MPR of the coronary arteries (LAD and CX). Bottom row, left: Iodine image. The iodine image shows homogeneous iodine distribution without perfusion defects in the myocardium. Bottom row, right: Virtual non-contrast image. Contrast agent is efficiently removed. All images were derived from the same scan.
Courtesy of the Institute of the Diagnostic Radiology, Mannheim University, Germany.

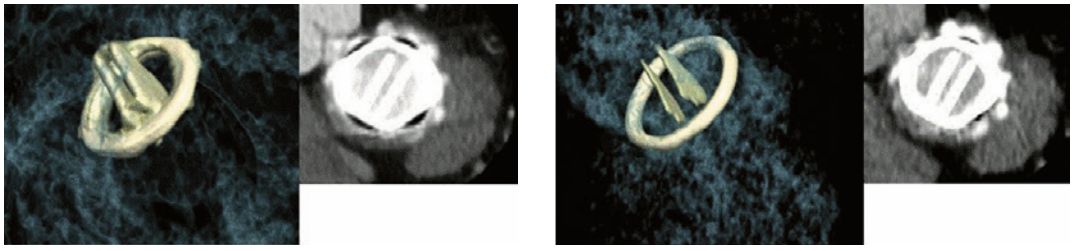

Mixed image | Monoenergetic Plus 170 keV

Figure 61: ECG-triggered “step-and-shoot” Dual Energy cardiac CT acquisition to reduce metal artifacts in an artificial valve. 90 kV / 150 Sn kV. Left: Mixed image corresponding to a standard 120 kV acquisition. Right: Virtual monoenergetic image at 170 keV. Metal artifacts are significantly reduced.
Courtesy of the Medical University of South Carolina, Charleston, SC, USA.

One main advantage of Dual Source CT technology compared with other vendor solutions is the ability to perform a fully dose-modulated Dual Energy scan without additional dose penalties. Several studies with SOMATOM Definition Flash have demonstrated dose neutrality (see Schenzle et al., 2010, Uhrig et al., 2016) when using Dual Energy in clinical routine.

7. Extended scan range and lower radiation dose for 4D angiographic studies and volume perfusion CT

SOMATOM Force offers an Adaptive 4D Spiral mode for acquiring dynamic CT data, for example for time-resolved CT angiographic studies or for volume perfusion CT. The scan mode is based on a periodic z-movement of the patient table during spiral data acquisition.

Dynamic CT scanning with an area detector is practically limited to a scan range equivalent to the z-axis coverage of the detector, e.g., 16 cm. The Adaptive 4D Spiral is more flexible in this respect. On SOMATOM Force, with detector z-axis coverage of 57.6 mm and 0.25 s gantry rotation time, a variety of different scan protocols is available. These range from 114 – 224 mm z-axis coverage at 1.5 s temporal resolution, to 800 mm scan range at 3.0 s temporal resolution. In this case, temporal resolution means the time between two subsequent acquisitions at the center of the scan range.

Table 2 gives an overview of the available scan techniques:

SubMode	Collimation	Detector width mm	N rot	Rotation time s	4DR length mm	4DR time s
PerfBrain	96*0.6	57.6	2	0.250	114	1.50
Perfusion1	96*0.6	57.6	2	0.250	114	1.50
Perfusion1	96*0.6	57.6	1	0.250	176	1.50
Perfusion1	96*0.6	57.6	1	0.250	224	1.50
Perfusion2	96*0.6	57.6	1	0.250	265	2.00
Perfusion2	96*0.6	57.6	1	0.250	340	2.00
Perfusion2	96*0.6	57.6	1	0.250	454	2.50
FastCTA	96*0.6	57.6	1	0.250	630	2.50
FastCTA	96*0.6	57.6	1	0.250	800	3.00
HeadAng	96*0.6	57.6	1	0.250	224	1.50
HeadAng	96*0.6	57.6	1	0.250	281	1.75
HeadAng	96*0.6	57.6	1	0.250	339	2.00
HeadAng	96*0.6	57.6	1	0.250	396	2.25
HeadAng	96*0.6	57.6	1	0.250	454	2.50
HeadAng	96*0.6	57.6	1	0.250	511	2.75
HeadAng	96*0.6	57.6	1	0.250	569	3.00

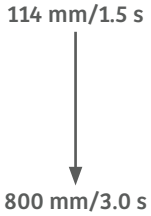

Table 2: Dynamic volume scanning using the Adaptive 4D Spiral – available scan protocols on SOMATOM Force. The left column indicates the intended clinical use.

The flexible z-axis coverage (114 mm – 800 mm) of the Adaptive 4D Spiral enables 4D angiographic studies of the brain, the carotid arteries, the aorta, and the legs.

With a maximum scan range of 800 mm and 70 kV X-ray tube voltage, time-resolved CTA of the peripheral arteries of the leg is feasible at a very low radiation dose. Delayed-contrast inflow can be differentiated from total stenosis, which is relevant for the management of the patient but may be misdiagnosed in single phase CTA examinations. In contrast to dynamic MR angiography, calcifications in the arteries are visible at high spatial resolution. This is beneficial for intervention and surgery planning. Fig. 62 shows a clinical example of a dynamic CTA examination of the legs.

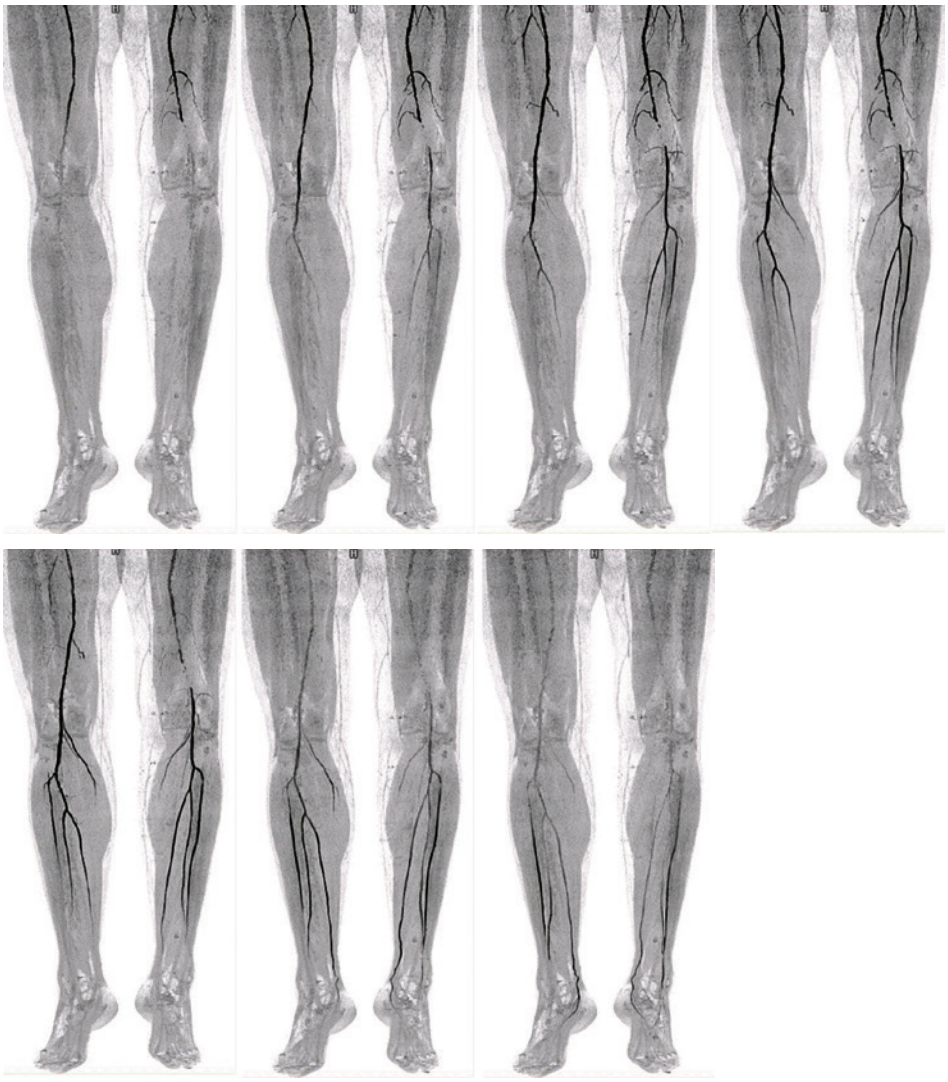

Figure 62: Dynamic CT angiographic study of the legs using the Adaptive 4D Spiral. Scan range 800 mm, 7 runs with a temporal resolution of 3.0 s, 70 kV.
Courtesy of the Clinical Innovation Center, Mayo Clinic Rochester, Minnesota, USA.

Volume perfusion CT of the body, for example for tumor perfusion studies, benefits from the significantly increased power reserves of the Vectron X-ray tube at low kV and the reduced electronic noise of the Stellar^{Infinity} detector compared with conventional detector designs. Body perfusion CT, with scan ranges from 114 mm to 454 mm, can routinely be performed at 80 kV X-ray tube voltage. The radiation dose for the patient is reduced by about 50% compared with the standard 100 kV protocol that had to be used with previous CT technology due to the limited tube power at 80 kV and increased image noise at low dose levels caused by electronic noise (Klotz et al. see Fig. 63).

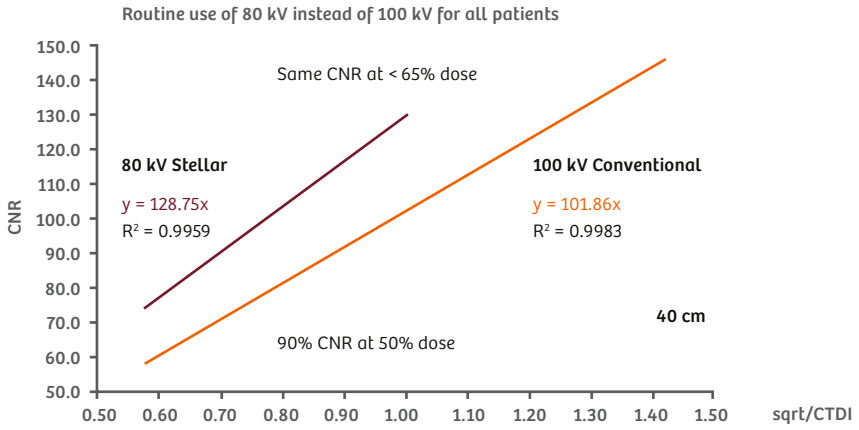

Figure 63: Iodine contrast-to-noise ratio (CNR) in a 40 cm water phantom as a function of the square-root of the radiation dose. The Stellar detector provides 90% of the CNR of a conventional 100 kV perfusion examination at 80 kV and at half the radiation dose for the patient. Sufficient power reserves with the Vectron tube enable the routine use of 80 kV for body perfusion examinations in all patients.

Fig. 64 shows a clinical example of a body perfusion examination for differential tumor diagnosis and follow-up. The radiation dose for 17.6 cm dynamic z-axis coverage at 80 kV tube voltage was about 14 mSv.

From a body volume perfusion scan, the vascular morphology and function in the scan region can be obtained as add-on information, see.

For ECG-triggered dynamic perfusion examinations of the heart, SOMATOM Force is equipped with a special ECG-triggered sequential shuttle mode to cover the entire myocardium with good temporal resolution at a low radiation dose.

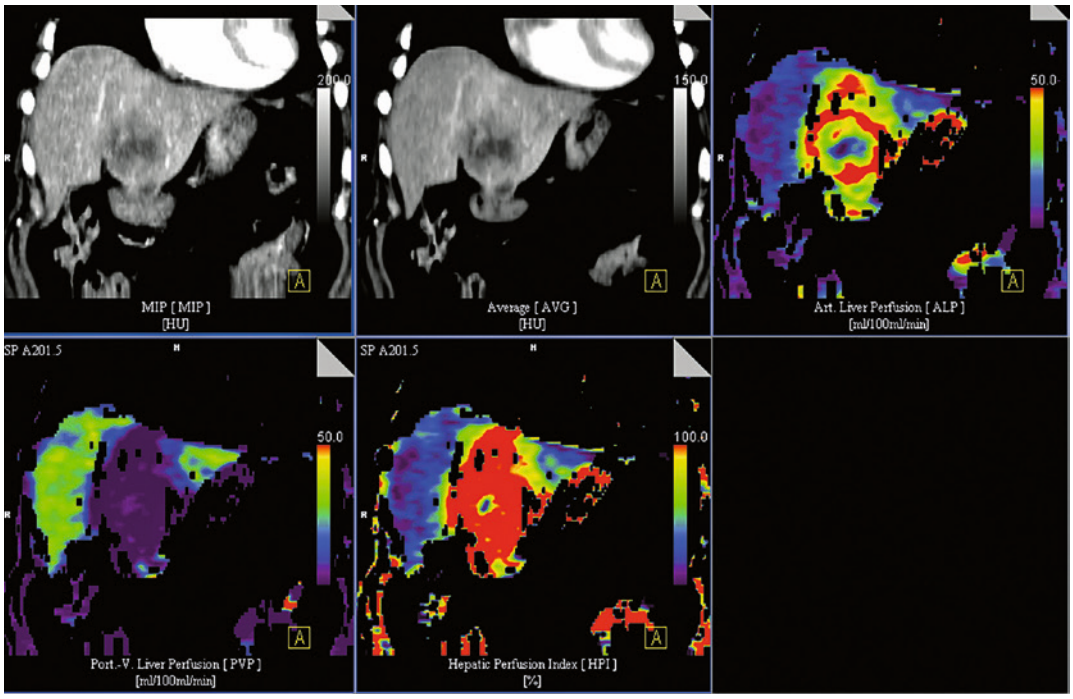

Figure 64: Volume perfusion study using the Adaptive 4D Spiral on SOMATOM Force in a patient with a large hypervascular liver tumor: 17.6 cm z-axis coverage, 80 kV X-ray tube voltage, effective radiation dose ~ 14 mSv. The tumor shows increased perfusion in the arterial phase (top row, right), and no remaining perfusion in the portal venous phase (bottom row, left).
Courtesy of the Institute of the Diagnostic Radiology, Mannheim University, Germany.

Figure 65: Dynamic CTA derived from a volume perfusion CT scan on SOMATOM Force: 17.6 cm z-axis coverage, 80 kV X-ray tube voltage, effective radiation dose ~ 12 mSv. Courtesy of University Hospital Zurich, Switzerland.

Myocardial perfusion imaging with SPECT/CT or with PET/CT is a mainstay in clinical practice for the diagnostic assessment of downstream, flow-limiting effects of epicardial lesions during hyperemic flows and for the risk stratification of patients with known or suspected coronary artery disease (CAD).

In patients with multivessel CAD, the relative distribution of radiotracer uptake in the left ventricular myocardium during stress and rest accurately identifies flow-limiting epicardial lesions or the most advanced, so-called culprit, lesion.

Often, less severe obstructive CAD lesions may go undetected or underdiagnosed. The concurrent ability of PET/CT with radiotracer kinetic modeling to determine myocardial blood flow (MBF) in absolute terms (mL/g/min) at rest and during vasomotor stress allows the computation of regional myocardial flow reserve (MFR) as an adjunct to the visual interpretation of myocardial perfusion studies.

Coronary computed tomography angiography (CTA) has been shown by several multicenter trials to have excellent diagnostic accuracy in the detection and exclusion of significant coronary stenosis. However, a major limitation of coronary CTA is that the physiological significance of the identified stenotic lesions is often unknown and over-estimated. Dynamic myocardial CT stress perfusion (CTP) is a new examination technique that provides both anatomic and physiological information. It was first commercially introduced with DSCT (SOMATOM Definition Flash) in 2009 (Bastarrika et al., 2010 and Mahnken et al., 2010). Mahnken et al. concluded that DSCT facilitates quantitative heart perfusion imaging at rest as well as under stress conditions, with a continuous infusion of adenosine (240 mg/kg/min) as demonstrated in Fig. 63. Dynamic stress perfusion CT has the potential to identify inducible (reversible) myocardial ischemia and to overcome a key limitation of cardiac CT – the mere morphological assessment of coronary artery stenosis. Ho et al. have demonstrated that the selection of patients for coronary revascularization is best performed by identifying inducible myocardial ischemia (Ho et al., 2010).

With SOMATOM Definition Flash, a scan length of 73 mm can be covered at a temporal resolution of up to 75 ms. With precise patient positioning and end-systolic triggering, the relevant area of the myocardium can be dynamically scanned. The ~ 30 s examination requires effective radiation doses of about 6 to 11 mSv (Ho et al., 2010).

In the meantime, multiple single-center studies have established the feasibility of stress myocardial CTP. Furthermore, it has been illustrated that a combined CTA/CTP protocol improves the diagnostic accuracy for detecting hemodynamically relevant stenosis compared with CTA alone.

In future, the ability to assess dynamic myocardial perfusion easily using CT imaging may improve diagnostic accuracy in coronary artery disease, and may have the potential to replace current nuclear medicine techniques. Varga-Szemes et al. (2015) have shown that dynamic myocardial perfusion is at present only available with Dual Source CT technology. SOMATOM Force provides a scan length of up to 105 mm (with dynamic acquisition in sequentially ECG-triggered mode, 2 x 96 x 0.6 mm collimation) for myocardial perfusion scanning, enabling full coverage of the myocardium. The improved temporal resolution of 66 ms with this scan mode is essential for increased clinical robustness at higher heart rates, in particular after inducing stress, see the clinical example in.

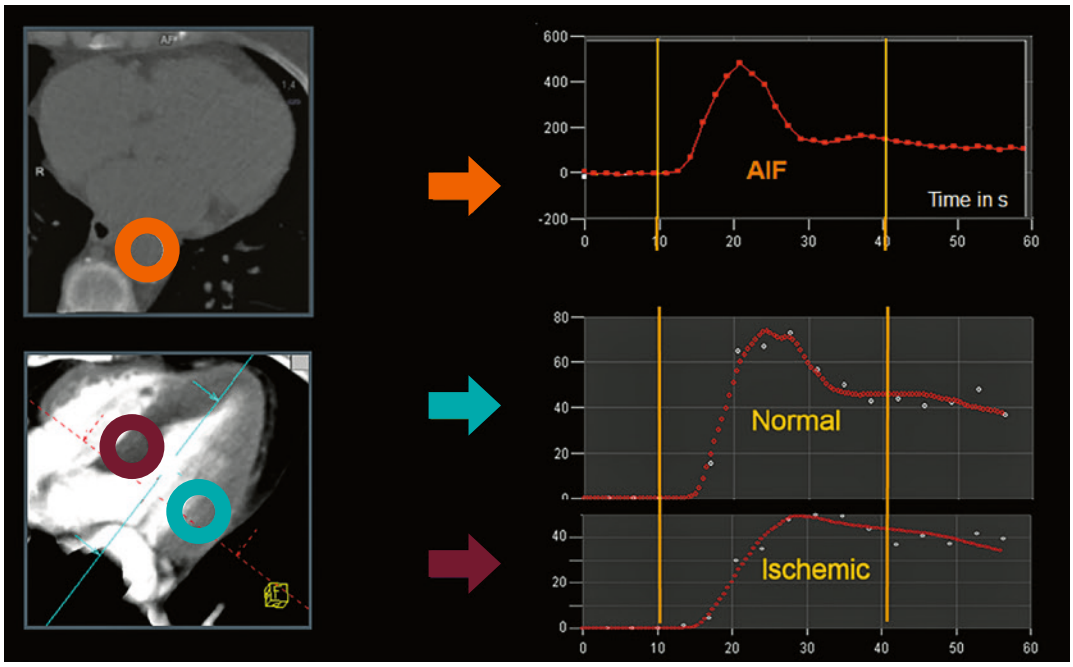

Figure 66: Basic measurement parameters in dynamic quantitative myocardial perfusion imaging with SOMATOM Force. The top curve, measured in the orange ROI, displays the arterial input function (AIF). The curve in the middle, measured in the green ROI, displays a normal blood flow. The curve at the bottom, measured in the purple ROI, displays an ischemic area in the myocardial wall.

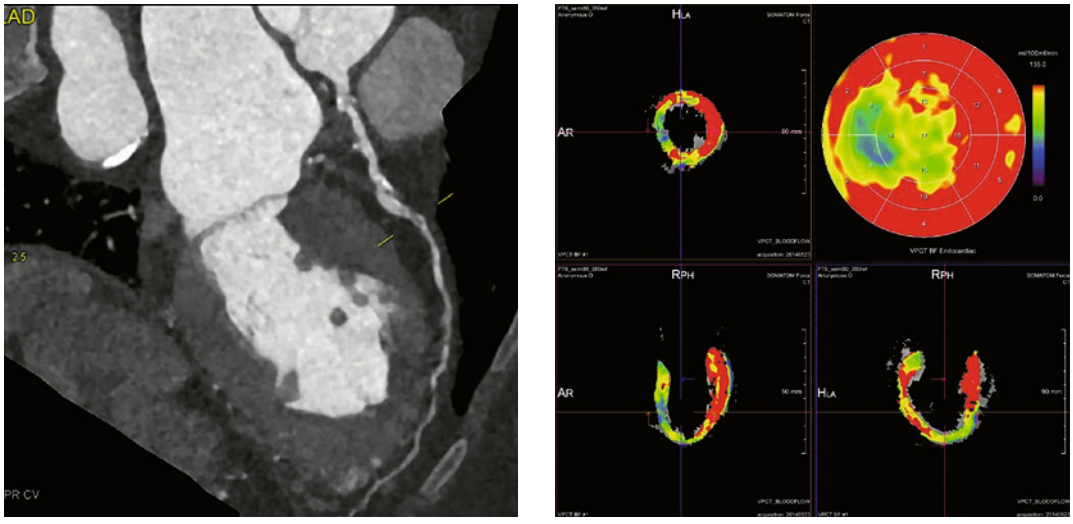

Figure 67: Prospectively triggered Turbo Flash coronary CTA with SOMATOM Force (80 kV / 117 mAs, 4.4 mSv) in a patient with known coronary artery disease shows intermediate – to high-grade LAD stenosis (left). Dynamic CT perfusion study of the whole myocardium, scan range 105 mm (right). The polar plot analysis shows reduced blood flow in the mid-anteroseptal to inferoseptal wall.
Courtesy of the Erasmus Medical Center, Rotterdam, The Netherlands.

Literature

Selected SOMATOM Force publications

Beeres. (2016) Beeres M, Trommer J, Frellesen C, Nour-Eldin NE, Scholtz JE, Herrmann E, Vogl TJ, Wichmann JL. Evaluation of different keV-settings in dual-energy CT angiography of the aorta using advanced image-based virtual monoenergetic imaging. Int J Cardiovasc Imaging, 2016 Jan;32(1):137-44

Bittner. (2016) Bittner DO, Arnold M, Klinghammer L, Schubaeck A, Hell MM, Muschiol G, Gauss S, Lell M, Uder M, Hoffmann U, Achenbach S, Marwan M. Contrast volume reduction using third generation dual source computed tomography for the evaluation of patients prior to transcatheter aortic valve implantation Eur Radiol. 2016 Mar 19 [Epub ahead of publication]

Dewes. (2016) Dewes P, Frellesen C, Scholtz JE, Fischer S, Vogl TJ, Bauer RW, Schulz B. Low-dose abdominal computed tomography for detection of urinary stone disease – Impact of additional spectral shaping of the X-ray beam on image quality and dose parameters. Eur J Radiol. 2016 jun;85(6):1058-62.

Duan. (2015) Duan X, Li Z, Yu L, Leng S, Halaweish AF, Fletcher JG, McCollough CH. Characterization of Urinary Stone Composition by Use of Third-Generation Dual-Source Dual-Energy CT With Increased Spectral Separation. AJR Am J Roentgenol. 2015 Dec;205(6):1203-7.

Frellesen. (2015) Frellesen C, Freia F, Hardie A, Wichmann J, De Cecco, CN, Schoepf J, Kerl M, Schulz B, Hammerstingl R, Vogl T, Bauer R. Dual-energy CT of the pancreas: improved carcinoma-to-pancreas contrast with a noiseoptimized monoenergetic reconstruction algorithm. Eur J Radiol. 2015; [Epub ahead of publication]

Gassenmaier. (2014) Gassenmaier T, Petri N, Allmendinger T, Flohr T, et al. Next generation coronary CT angiography: in vitro evaluation of 27 coronary stents. Eur Rad 24(11), p.2953-2961.

Goenka. (2014) Goenka AH, Herts BR, Obuchowski NA, et al. Effect of reduced radiation exposure and iterative reconstruction on Detection of Low-Contrast Low-Attenuation Lesions in an Anthropomorphic Liver Phantom: An 18-Reader Study. Radiology 272, p.154-163.

Gordic. (2014) Gordic S, Husarik D, Desbiolles L, Leschka S, Frauenfelder T, Alkadhi H. High-pitch coronary CT angiography with third generation dual-source CT: limits of heart rate. Int J Cardiovasc Imaging, Epub May 11, 2014.

Gordic. (2014) Gordic S, Morsbach F, Schmidt B, Allmendinger T, et al. Ultralow-Dose Chest Computed Tomography for Pulmonary Nodule Detection: First Performance Evaluation of Single Energy Scanning With Spectral Shaping. Inv Rad 49(7); p.465-473.

A full list of SOMATOM Force publications is available by Siemens Healthineers. Please contact your local Siemens Healthineers organization for further details.

Hagelstein. (2015) Hagelstein C, Henzler T, Haubenreisser H, Meyer M, Sudarski S, Schoenberg SO, Neff KW, Weis M. Ultra-high pitch chest computed tomography at 70 kVp tube voltage in an anthropomorphic pediatric phantom and non-sedated pediatric patients: Initial experience with 3rd generation dual-source CT. Z Med Phys. 2015 Dec 15.

Hardie. (2015) Hardie AD, Picard MM, Camp ER, Perry JD, Suranyi P, De Cecco CN, Schoepf UJ, Wichmann JL. Application of an Advanced Image-Based Virtual Monoenergetic Reconstruction of Dual Source Dual-Energy CT Data at Low keV Increases Image Quality for Routine Pancreas Imaging. J Comput Assist Tomogr. 2015 Jul;20

Haubenreisser. (2015) Haubenreisser H, Meyer M, Sudarski S, Allmendinger T, Schoenberg S, Henzler T. Unenhanced third-generation dual-source chest CT using a tin filter for spectral shaping at 100 kVp. Eur J Radiol (2015) Aug;84(8):1608-13

Higashigaito. (2016) Higashigaito K, Schmid T, Puippe G, Morsbach F, Lachat M, Seifert B, Pfammatter T, Alkadhi H, Husarik DB. CT Angiography of the Aorta: Prospective Evaluation of Individualized Low-Volume Contrast Media Protocols. Radiology. 2016 Mar 2:151982 [Epub ahead of print]

Kaup. (2016) Kaup M, Wichmann JL, Scholtz JE, Beeres M, Kromen W, Albrecht MH, Lehnert T, Boettcher M, Vogl TJ, Bauer RW. Dual-Energy CT-based Display of Bone Marrow Edema in Osteoporotic Vertebral Compression Fractures: Impact on Diagnostic Accuracy of Radiologists with Varying Levels of Experience in Correlation to MR Imaging. Invest Radiol., 2015 Mar;50(3):161-7

Krauss. (2015) Krauss B, Grant KL, Schmidt BT, Flohr TG. The importance of spectral separation: an assessment of dual-energy spectral separation for quantitative ability and dose efficiency. Invest Radiol Feb, 2015;50(2):114-8.

Lell. (2015) Lell MM, May MS, Brand M, Eller A, Bruder T, Hofmann E, Uder M, Wuest M. Imaging the Parasinus Region with a Third-Generation Dual Source CT and the Effect of Tin Filtration on Image Quality and Dose. AJNR Am J Neuroradiol. 2015 Jul,36(7):1225-30

Martini. (2016) Martini K, Barth BK, Nguyen-Kim TD, Baumueller S, Alkadhi H, Frauenfelder T. Evaluation of pulmonary nodules and infection on chest CT with radiation dose equivalent to chest radiography: Prospective intra-individual comparison study to standard dose CT Eur J Radiol. 2016 Feb;85(2):360-5.

Mangold S, Wichmann JL, Schoepf UJ, Litwin SE, Canstein C, Varga-Szemes A, Muscogiuri G, Fuller SR, Stubenrauch AC, Nikolaou K, De Cecco CN. Coronary CT angiography in obese patients using 3rd generation dual-source CT: effect of body mass index on image quality. Eur Radiol. 2016 Sep;26(9):2937-46

Meinel. (2014) Meinel FG, Canstein C, Schoepf UJ, Sedlmaier M, Schmidt B, Harris BS, Flohr TG, De Cecco CN. Image quality and radiation dose of low tube voltage 3(rd) generation dual-source coronary CT angiography in obese patients: a phantom study. Eur Radiol, 24(7):1643-50.

Meyer. (2015) Meyer M, Haubenreisser H, Raupach R, Schmidt B, et al. Initial results of a new generation Dual Source CT system using only an in-plane comb filter for ultra-high resolution temporal bone imaging. Eur Rad 25(1), p. 178-185.

Meyer. (2014) Meyer M, Haubenreisser H, Schoepf UJ, et al. Closing in on the K Edge: Coronary CT Angiography at 100, 80, and 70 kV – Initial Comparison of a Second- versus a Third-Generation Dual-Source CT System. Radiology, May 31:140244. [Epub ahead of print].

Morsbach. (2014) Morbach F, Gordic S, Desbiolles L, Husarik D, Frauenfelder T et al. Performance of turbo high-pitch dual-source CT for coronary CTangiography: first ex vivo and patient experience. Eur Radiol, epub May 17, 2014.

Newell. (2015) Newell JD, Fuld M, Allmendinger T, Sieren JP, et al. Very Low-Dose (0.15 mGy) Chest CT Protocols Using the COPDGene 2 Test Object and a Third-Generation Dual-Source CT Scanner With Corresponding Third-Generation Iterative Reconstruction Software. Inv Rad 50(1), p.40-45.

Rompel. (2016) Rompel O, Glöckler M, Janka R, Dittrich S, Cesnjevar R, Lell MM, Uder M, Hammon M. Third-generation dual-source 70-kVp chest CT angiography with advanced iterative reconstruction in young children: image quality and radiation dose reduction. Pediatr Radiol. 2016 Apr;46(4):462-72

Schaller. (2016) Schaller F, Sedlmair M, Raupach R, Uder M, Lell M. Noise Reduction in Abdominal Computed Tomography Applying Iterative Reconstruction (ADMIRE). Acad Radiol. 2016;Jun 15

Schenzle. (2010) Schenzle JC, Sommer WH, Neumaier K, Michalski G, Lechel U, Nikolaou K, Becker CR, Reiser MF, Johnson TR. Dual energy CT of the chest: how about the dose? Invest Radiol Jun 2010, 45(6):347-53.

Scholtz. (2015) Scholtz JE, Wichmann JL, Hüsers K, Albrecht MH, Beeres M, Bauer RW, Vogl TJ, Bodelle B. Third-generation dual-source CT of the neck using automated tube voltage adaptation in combination with advanced modeled iterative reconstruction: evaluation of image quality and radiation dose. Eur Radiol. 2015 Nov 11.

Solomon. (2015) Solomon J, Ramirez-Giraldo JC, Mileto A, Samei E. Diagnostic Performance of an Advanced Modeled Iterative Reconstruction Algorithm for Low-Contrast Detectability on a Third-Generation Dual-Source MDCT Scanner: Potential for Radiation Dose Reduction in a Multireader Study. Radiology, 2015, In Press.

Sudarski. (2015) Sudarski S, Hagelstein C, Weis M, Schoenberg SO, Apfaltrer P. Dual-energy snap-shot perfusion CT in suspect pulmonary nodules and masses and for lung cancer staging. Eur J Radiol. 2015 Dec;84(12):2393-400

Uhrig. (2016) Uhrig M, Simons D, Kachelrieß M, Pisana F, Kuchenbecker S, Schlemmer HP. Advanced abdominal imaging with dual energy CT is feasible without increasing radiation dose. Cancer Imaging. 2016 Jun 21;16(1):15

Wenz. (2015) Wenz H, Maros ME, Meyer M, Förster A, Haubenreisser H, Kurth S, Schoenberg SO, Flohr T, Leidecker C, Groden C, Scharf J, Henzler T. Image Quality of 3rd Generation Spiral Cranial Dual-Source CT in Combination with an Advanced Model Iterative Reconstruction Technique: A Prospective Intra-Individual Comparison Study to Standard Sequential Cranial CT Using Identical Radiation Dose PLoS One. 2015 Aug 19;10(8):e0136054.

Wortman. (2016) Wortman JR, Bunch PM, Fulwadhva UP, Bonci GA, Sodickson AD. Dual-Energy CT of Incidental Findings in the Abdomen: Can We Reduce the Need for Follow-Up Imaging? AJR AM J Roentgenol. 2016 Jul 6:W1-W11

Literature

Other publications

Alkadhi. (2010) Low-dose, 128-slice, dual-source CT coronary angiography: accuracy and radiation dose of the high-pitch and the step-and-shoot mode. Heart, 933-8.

Andre. (2013) André F1, Korosoglou G, Hosch W, Giannitsis E, Kauczor HU, Katus HA, Steen H. Performance of dual-source versus 256-slice multi-slice CT in the evaluation of 16 coronary artery stents. Eur J Radiol, 82(4): 601-7.

Azzalini. (2014) Azzalini L, Abbara S, Ghoshhajra BB. Ultra-Low Contrast Computed Tomographic Angiography (CTA) With 20-mL Total Dose for Transcatheter Aortic Valve Implantation (TAVI) Planning. JCAT, 38(1): 105-9.

Barrett. (2012) Barrett T1, Bowden DJ, Shaida N, Godfrey EM, Taylor A, Lomas DJ, Shaw AS. Virtual unenhanced second generation dual-source CT of the liver: is it time to discard the conventional unenhanced phase? Eur J Radiol. 2012 Jul;81(7):1438-45.

Bastarrika, G. (2010) Adenosine-stress dynamic myocardial CT perfusion imaging: initial clinical experience. Invest Radiol, 306-13.

Beister. (2012) Beister M, Kolditz D, Kalender W. Iterative reconstruction methods in X-ray CT. Phys Med 28(2), p. 94-108.

Bischoff. (2013) Bischoff B, Meinel FG, Reiser M, Becker HC. Novel single-source high-pitch protocol for CT angiography of the aorta: comparison to high-pitch dual-source protocol in the context of TAVI planning. Int J Cardiovasc Imaging, 29(5): 1159-65.

Blanke. (2010) Blanke P, Bulla S, Baumann T e t al. Thoracic aorta: prospective electrocardiographically triggered CT angiography with dual-source CT – feasibility, image quality, and dose reduction. Radiology, 255:207-17.

Bruder. (2011) Bruder H, Raupach R, Sunnegardh J, et al. Adaptive Iterative Reconstruction. Proc of SPIE Vol. 79610J1-12.

Cao. (2014) Cao JX, Wang YM, Lu JG, Zhang Y et al. Radiation and contrast agent doses reductions by using 80-kV tube voltage in coronary computed tomographic angiography: a comparative study. Eur J Radiol, 83(2): 309-314.

Corcuera. (2014) Corcuera-Solano I, Doshia AH, Noora A, Tanenbaum LN. Repeated Head CT in the Neurosurgical Intensive Care Unit: Feasibility of Sinogram-Affirmed Iterative Reconstruction–Based Ultra-Low-Dose CT for Surveillance. AJNR 35, p.1281-1287.

Duan. (2013) Duan X, Wang J, Leng S, Schmidt B, Allmendinger T, Grant K, Flohr T, McCollough C H. Electronic Noise in CT Detectors: Impact on Image Noise and Artifacts. AJR, 201: W626-W632.

Fletcher. (2013) Fletcher JG, Krueger WR, Hough DM, et al. Pilot study of detection, radiologist confidence and image quality with sinogram-affirmed iterative reconstruction at half-routine dose level. J Comput Assit Tomogr 37(2): 203-211.

Flohr. (2009) Flohr T, Leng S, Yu L, Allmendinger T, Bruder H et al. Dual-source spiral CT with pitch up to 3.2 and 75 ms temporal resolution: Image reconstruction and assessment of image quality. Med Phys, 36(12): 5641-5653.

Gordic. (2014) Gordic S, Desbiolles L, Stolzmann P, Gantner L, et al. Advanced modelled iterative reconstruction for abdominal CT: Qualitative and quantitative evaluation. Clin Rad 69(12); e497-e504.

Grant. (2012) Grant K, and Raupach R. SAFIRE: Sinogram Affirmed Iterative Reconstruction, White Paper. Siemens Healthineers.

Grant. (2010) Grant K, and Flohr T. Iterative Reconstruction in Image Space (IRIS): White Paper. Siemens Healthineers; A9115-101492.

Grant. (2014) Grant KL, Flohr TG, Krauss B et al. Assessment of an Advanced Image-Based Technique to Calculate Virtual Monoenergetic CT Images From a Dual-Energy Examination to Improve Contrast-To-Noise Ratio in Examinations Using Iodinated Contrast Media. Invest Radiol, Apr 4. [Epub ahead of print].

Hausleiter. (2009) Hausleiter J, Meyer T, Hermann F et al. Estimated Radiation Dose Associated With Cardiac CT Angiography. JAMA, 301(5): 500-507.

Hausleiter. (2010) Hausleiter J, Martinoff S, Hadamitzky M et al. Image Quality and Radiation Exposure with a Low Tube Voltage Protocol for Coronary CT Angiography-Results of the Protection II trial. JACC: Cardiovascular Imaging, 3(11): 1113-1123.

Hausleiter. (2012) Hausleiter J, Meyer T, Martuscelli E. Image Quality and Radiation Exposure with Prospectively ECG-Triggered Axial Scanning for Coronary CT Angiography-The Multicenter, Multivendor, Randomized PROTECTION-III Study. JACC: Cardiovascular Imaging, 5(5): 484-493.

Ho, K. (2010) Stress and rest dynamic myocardial perfusion imaging by evaluation of complete time attenuation curves with dual-source CT. JACC Cardiovasc Imaging, 811-20.

Klotz. (2013) Klotz E, Haberland U, Schmidt B. Performance evaluation of a new CT detector with minimal electronic noise for low dose abdominal perfusion imaging. ECR, B-0240.

Komatsu. (2013) Komatsu S et al. Coronary Computed Tomography angiography using ultra-low-dose contrast media: radiation dose and image quality. Int J Cardiovasc Imaging, 29(6): 1335-40.

Lee. (2011) Lee SJ, Park SH, Kim AY, et al. A prospective comparison of standard-dose CT enterography and 50% reduced-dose CT enterography with and without noise reduction for evaluating Chrohn disease. AJR Am J Roentgenol. 197(1), p. 50-57.

Mahnken. (2010) Quantitative whole heart stress perfusion CT imaging as noninvasive assessment of hemodynamics in coronary artery stenosis: preliminary animal experience. Invest Radiol.

Maintz. (2009) Maintz D, Burg MC, Seifarth H, Bunck AC, Ozgün M, Fischbach R, Jürgens KU, Heindel W. Update on multidetector coronary CT angiography of coronary stents: in vitro evaluation of 29 different stent types with dual-source CT. Eur Radiol, 19(1):42-9.

Marti. (2012) Marti G, Alvarez-Sala R, Soto J A. Acute lower intestinal bleeding: feasibility and diagnostic performance of CT angiography. Radiology, 262: 109- 16.

McCollough. (2009) McCollough CH, Primak AN, Braun N, Kofler J, Yu L, Christner J. Strategies for Reducing Radiation Dose in CT. Radiol Clin North Am, 47(1): 27-40.

McCollough. (2013) McCollough C H, Leng S, Sunnegardh J, Vrieze T J, Yu L, Lane J, Raupach R, Stierstorfer K, Flohr T. Spatial resolution improvement and dose reduction potential for inner ear CT imaging. Med Phys, 40(6).

Morsbach. (2013) Morsbach F, Desbiolles L, Plass A, Leschka S, Schmidt S, Falk V, Alkadhi H, Stolzmann P. Stenosis Quantification in Coronary CT Angiography-Impact of an Integrated Circuit Detector With Iterative Reconstruction. Invest Radiol, 48(1):1-9.

Pontana. (2013) Pontana F, Pagniez J, Duhamel A., et al. Reduced-dose low-voltage chest CT angiography with Sinogram-affirmed Iterative Reconstruction. Radiology 267(2).

Primak. (2009) Primak A N, Ramirez Giraldo JC, Liu X, Yu L, McCollough CH. Improved dual-energy material discrimination for dual-source CT by means of additional spectral filtration. Med Phys, 36(4):1359-69.

Renker. (2011) Renker M, Ramachandra A, Schoefp UJ, et al. Iterative image reconstruction techniques: Applications for cardiac CT. J Cardiovasc Comput Tomogr 5(4), p. 225-230.

Schenzle. (2011) Schenzle JC1, Sommer WH, Neumaier K, Michalski G, Lechel U, Nikolaou K, Becker CR, Reiser MF, Johnson TR. Dual energy CT of the chest: how about the dose? Invest Radiol. 2010 Jun;45(6):347-53.

Schindera. (2010) Schindera S T, Tock I, Marin D. Effect of beam hardening on arterial enhancement in thoracoabdominal CT angiography with increasing patient size: an in vitro and in vivo study. Radiology, 256: 528-35.

Siegel. (2004) Siegel MJ, Schmidt B, Bradley D, Suess C, Hildebolt C. Radiation Dose and Image Quality in Pediatric CT: Effect of Technical Factors and Phantom Size and Shape. Radiology, 233(2): 515-22.

Steinwender. (2009) Steinwender C, Schützenberger W, Fellner F et al. 64-detector CT angiography in renal artery stent evaluation: prospective comparison with selective catheter angiography. Radiology, 252:299-305.

Tricarico. (2013) Tricarico F, Hlavacek AM, Schoepf UJ, et al. Cardiovascular CT angiography in neonates and children: Image quality and potential for radiation dose reduction with iterative image reconstruction techniques. Eur Rad 23, p. 1306-1315.

Varga-Szemes A, Meinel F, De Cecco C, Fuller S, Bayer II R, Schoepf J. CT Myocardial Perfusion Imaging. AJR. 2015; 204: 487-497

Vliegenthart. (2012) Vliegenthart R, Pelgrim G J, Ebersberger U et al. Dual-Energy CT of the Heart. AJR, 199: S54-S63.

Wielandner A, Beitzke D, Schernthaner R, Wolf F, Langenberger C, Stadler A, Loewe C. Is ECG Triggering for Motion Artifact Reduction in Dual-Source CT Angiographies of the Ascending Aorta still required in times of High-Pitch scanning? Br J Radiol. 2016 Jun 1:20160174.

Wuest. (2012) Wuest W, Anders K, Schuhbaeck A et al. Dual-source multidetector CT-angiography before Transcatheter Aortic Valve Implantation (TAVI) using a high-pitch spiral acquisition mode. Eur Radiol, 22(1): 51 -8.

Zhang. (2010) Zhang LJ, Peng J, Wu SY et al. Liver virtual non-enhanced CT with dual-source, dual-energy CT: a preliminary study. Eur Radiol, 20(9): 2257-64.

Notes

On account of certain regional limitations of sales rights and service availability, we cannot guarantee that all products included in this brochure are available through the Siemens Healthineers sales organization worldwide.

Availability and packaging may vary by country and are subject to change without prior notice. Some/All of the features and products described herein may not be available in the United States.

The information in this document contains general technical descriptions of specifications and options as well as standard and optional features which do not always have to be present in individual cases.

Siemens Healthineers reserves the right to modify the design, packaging, specifications, and options described herein without prior notice. Please contact your local Siemens Healthineers sales representative for the most current information.

Note: Any technical data contained in this document may vary within defined tolerances. Original images always lose a certain amount of detail when reproduced.

International version.
Not for distribution or use in the U.S.

Siemens Healthineers Headquarters
Siemens Healthcare GmbH
Henkestr. 127
91052 Erlangen, Germany
Phone: +49 9131 84-0
siemens-healthineers.com

Published by Siemens Healthcare GmbH · Order No. A91CT-02373-06C2-7600 · Printed in Germany · 5959 ·